ISSN: 2153-1285 Vol.1, No.2, October 2010

Scientific Research

Circuits and Systems

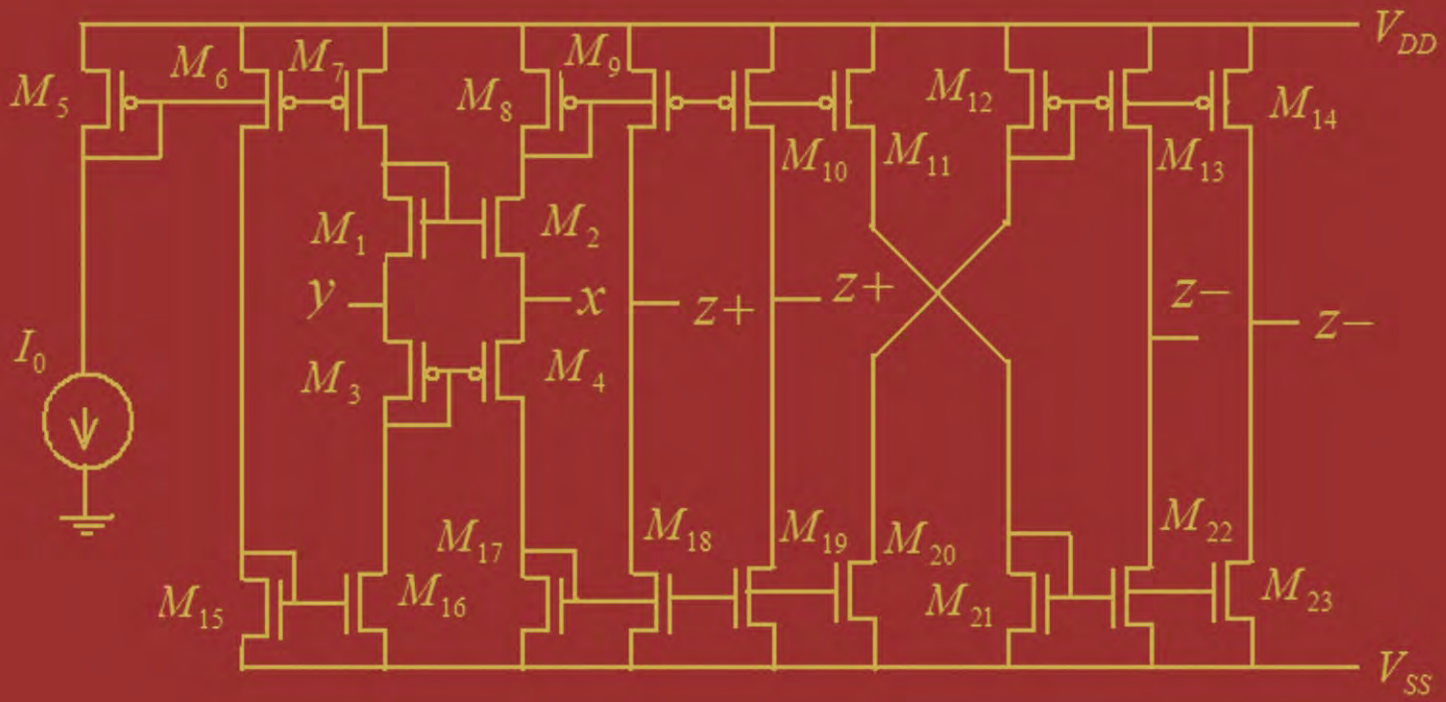

ISSN: 2153-1285

www.scirp.org/journal/cs

Journal Editorial Board

ISSN 2153-1285 (Print) ISSN 2153-1293 (Online)

http://www.scirp.org/journal/cs

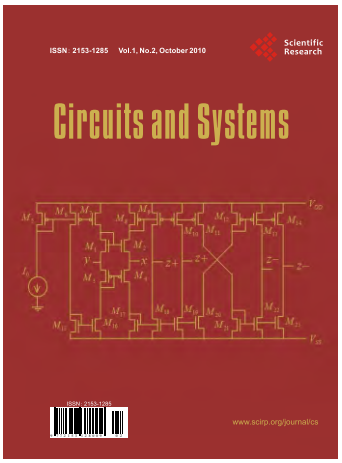

Call for Papers

Circuits and Systems

ISSN Print: 2153-1285 ISSN Online:2153-1293

http://www.scirp.org/journal/cs

Circuits and Systems is an international journal dedicated to the latest advancement of theories, methods and applications in Electronics, Circuits and Systems. The goal of this journal is to provide a platform for scientists and academicians all over the world to promote, share, and discuss various new issues and developments in different areas of electronics, circuits and systems.

Subject Coverage

All manuscripts must be prepared in English, and are subject to a rigorous and fair peer-review process. Accepted papers will immediately appear online followed by printed hard copy. The journal publishes original papers including but not limited to the following fields:

- Analog Signal Processing
- Biomedical Circuits and Systems
- Blind Signal Processing
- Cellular Neural Networks and Array Computing
- Circuits and Systems for Communications
- Computer-Aided Network Design
- Digital Signal Processing
- Graph Theory and Computing
- Life-Science Systems and Applications
- Live Demonstrations of Circuits and Systems
- Multimedia Systems and Applications
- Nanoelectronics and Gigascale Systems
- Neural Systems and Applications
- Nonlinear Circuits and Systems
- Power Systems and Power Electronic Circuits
- Sensory Systems
- Visual Signal Processing and Communications
- VLSI Systems and Applications

We are also interested in: 1) Short Reports 2-5 page papers where an author can either present an idea with theoretical background but has not yet completed the research needed for a complete paper or preliminary data; 2) Book Reviews Comments and critiques.

Notes for Intending Authors

Submitted papers should not have been previously published nor be currently under consideration for publication elsewhere. Paper submission will be handled electronically through the website. All papers are refereed through a peer review process. For more details about the submissions, please access the website.

Website and E-Mail

http://www.scirp.org/journal/cs E-mail:cs@scirp.org

Circuits and Systems, 2010, 1, 35-75
Published Online October 2010 in SciRes (http://www.SciRP.org/journal/cs).

TABLE OF CONTENTS

Volume 1 Number 2 **October 2010**

Circuits and Systems, **2010, 1, 35-75**
Published Online October 2010 in SciRes (http://www.SciRP.org/journal/cs/)

TABLE OF CONTENTS

Volume 1 Number 2 October 2010

The figure on the front cover is from the article published in Circuits and Systems, 2010, Vol. 1, No. 2, pp. 54-58 by Neeta Pandey and Sajal K. Paul.

Circuits and Systems

Journal Information

SUBSCRIPTIONS

The *Circuits and Systems* (Online at Scientific Research Publishing, www.SciRP.org) is published quarterly by Scientific Research Publishing, Inc., USA.

Subscription rates:

Print: $50 per copy.
To subscribe, please contact Journals Subscriptions Department, E-mail: sub@scirp.org

SERVICES

Advertisements
Advertisement Sales Department, E-mail: service@scirp.org

Reprints (minimum quantity 100 copies)
Reprints Co-ordinator, Scientific Research Publishing, Inc., USA.
E-mail: sub@scirp.org

COPYRIGHT

PRODUCTION INFORMATION

For manuscripts that have been accepted for publication, please contact:
E-mail: cs@scirp.org

Circuits and Systems, **2010, 1, 35-40**
doi:10.4236/cs.2010.12006 Published Online October 2010 (http://www.SciRP.org/journal/cs)

Universal Current-Controlled Current-Mode Biquad Filter Employing MO-CCCCTAs and Grounded Capacitors

Sajai Vir Singh[1], Sudhanshu Maheshwari[2], Durg Singh Chauhan[3]
[1]*Department of Electronics and Communications, Jaypee University of Information Technology, Waknaghat, India*
[2]*Department of Electronics Engineering, Z. H. College of Engineering and Technology, Aligarh Muslim University, Aligarh, India*
[3]*Department of Electrical Engineering, Institute of Technology, Banaras Hindu University, Varanasi, India*
E-mail: {*sajaivir, sudhanshu_maheshwari*}*@rediffmail.com, pdschauhan@gmail.com*
Received May 22, 2010; *revised July* 19, 2010; *accepted July* 23, 2010

Abstract

This paper presents a universal current-controlled current-mode biquad filter employing current controlled current conveyor trans-conductance amplifiers (CCCCTAs). The proposed filter employs only three MO-CCCCTAs and two grounded capacitors. The proposed filter can simultaneously realize low pass (LP), band pass (BP), high pass (HP), band reject (BR) and all pass (AP) responses in current form by choosing appropriate current output branches. In addition, the pole frequency and quality factor of the proposed filter circuit can be tuned independently and electronically over the wide range by adjusting the external bias currents. The circuit possesses low active and passive sensitivity performance. The validity of proposed filter is verified through PSPICE simulations.

Keywords: Biquad, Current-Mode, Universal Filter

1. Introduction

It is well accepted that universal biquad filter is a very important functional block which is widely used in various parts such as communication, measurement, instrumentation and control systems [1]. Because of the well known advantages such as reduced distortions, low input impedance, high output impedance, less sensitive to switching noise, better ESD immunity, high slew rate and larger bandwidth, the design and implementation of current-mode active filters using current-mode active elements [2] have become quite popular for wide variety of applications due to their inherent advantages over the voltage-mode counter parts. Recently, a new current-mode active element, namely the current controlled current conveyor trans-conductance amplifiers (CCCCTAs) has been introduced [3]. Its trans-conductance and parasitic resistance can be adjusted electronically, hence it does not need a resistor in practical applications. This device can be operated in both current and voltage-modes, providing flexibility. In addition, it can offer several advantages such as high slew rate, high speed, wider bandwidth and simpler implementation. All these advantages together, its current-mode operation makes the CCCCTA, a promising choice for realizing active filters [4]. During the last one decade and recent past a number of universal current-mode active filters have been reported in the literature [5-23], using different current-mode active elements. Unfortunately these reported current-mode filters [5-23] suffer from one or more of the following drawbacks:

1) Lack of electronic tunability [5,7,9,11,20].

2) Can not provide completely standard filter functions simultaneously [8,13,15,18,21-23].

3) Excessive use of active and/or passive elements [5,6,9, 11,12,14,16-19].

4) Can not provide explicit current outputs [8,13,15].

5) Pole frequency and quality factor can't be controlled orthogonally [8,10,22].

In this paper a new universal current-controlled current-mode biquad filter using three MO-CCCCTAs and two grounded capacitors is proposed. The proposed filter can simultaneously realize LP, BP, HP, BR and AP responses in current form. In addition, the pole frequency and quality factor of the proposed filter circuit can be tuned independently and electronically over the wide

range by adjusting the external bias currents. Both the active and passive sensitivities are less and no longer than one. The validity of proposed filter is verified through PSPICE, the industry standard tool.

2. Proposed Circuit

The CCCCTA properties can be described by the following equations

$$V_{Xi} = V_{Yi} + I_{Xi}R_{Xi} \quad , I_{Zi} = I_{Xi} \, , \quad I_{\pm O} = \pm g_{mi}V_{Zi} \tag{1}$$

where R_{Xi} and g_{mi} are the parasitic resistance at X terminal and transconductance of the i^{th} CCCCTA, respectively. R_{Xi} and g_{mi} depend upon the biasing currents I_{Bi} and I_{Si} of the CCCCTA, respectively. The schematic symbol of MO-CCCCTA is illustrated in **Figure 1**. For BJT model of MO-CCCCTA [3] shown in **Figure 2**, R_{Xi} and g_{mi} can be expressed as

$$R_{Xi} = \frac{V_T}{2I_{Bi}} \quad \text{and} \quad g_{mi} = \frac{I_{Si}}{2V_T} \tag{2}$$

The proposed current-mode universal filter is shown in **Figure 3**. It is based on three MO-CCCCTAs and two grounded capacitors. Routine analysis of proposed filter yields the circuit transfer functions $T_{LP}(s)$, $T_{BP}(s)$, $T_{HP}(s)$, $T_{BR}(s)$ and $T_{AP}(s)$ for the current outputs $I_{LP}(s)$, $I_{BP}(s)$, $I_{HP}(s)$, $I_{BR}(s)$ and $I_{AP}(s)$ and can be formulated as

$$T_{LP}(s) = \frac{I_{LP}(s)}{I_{in}(s)} = -g_{m1}R_{X1}\frac{g_{m2}}{s^2C_1C_2R_{X2} + sg_{m1}R_{X1}C_2 + g_{m2}} \tag{3}$$

$$T_{HP}(s) = \frac{I_{HP}(s)}{I_{in}(s)} = g_{m1}R_{X1}\frac{s^2C_1C_2R_{X2}}{s^2C_1C_2R_{X2} + sg_{m1}R_{X1}C_2 + g_{m2}} \tag{4}$$

$$T_{BP}(s) = \frac{I_{BP}(s)}{I_{in}(s)} = -g_{m1}R_{X1}\frac{\frac{sC_2g_{m3}R_{X3}}{2}}{s^2C_1C_2R_{X2} + sg_{m1}R_{X1}C_2 + g_{m2}} \tag{5}$$

$$T_{BR}(s) = \frac{I_{BR}(s)}{I_{in}(s)} = g_{m1}R_{X1}\frac{s^2C_1C_2R_{X2} + g_{m2}}{s^2C_1C_2R_{X2} + sg_{m1}R_{X1}C_2 + g_{m2}} \tag{6}$$

$$T_{AP}(s) = \frac{I_{AP}(s)}{I_{in}(s)} = -g_{m1}R_{X1}\frac{s^2C_1C_2R_{X2} - \frac{sC_2g_{m3}R_{X3}}{2} + g_{m2}}{s^2C_1C_2R_{X2} + sg_{m1}R_{X1}C_2 + g_{m2}} \tag{7}$$

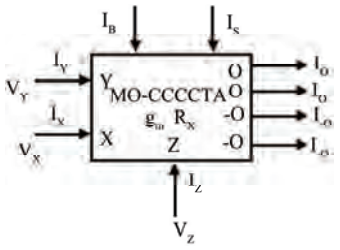

Figure 1. CCCCTA symbol.

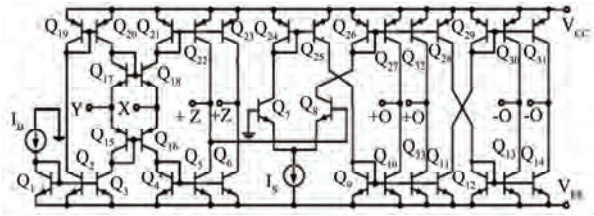

Figure 2. Internal topology of MO-CCCCTA.

It is noted from (7) that simple current matching condition is required to get AP response which is $I_{S3}I_{B1} = 2I_{S1}I_{B3}$. The pole frequency ($\omega_o$), the quality factor ($Q$) and Bandwidth ($BW$) ω_o/Q of each filter response can be expressed as

$$\omega_o = \left(\frac{g_{m2}}{C_1C_2R_{X2}}\right)^{\frac{1}{2}}, Q = \frac{1}{g_{m1}R_{X1}}\left(\frac{C_1R_{X2}g_{m2}}{C_2}\right)^{\frac{1}{2}},$$
$$BW = \frac{\omega_0}{Q} = \frac{g_{m1}R_{X1}}{C_1R_{X2}} \tag{8}$$

Substituting intrinsic resistances as depicted in (2), it yields

$$\omega_o = \frac{1}{V_T}\left(\frac{I_{S2}I_{B2}}{C_1C_2}\right)^{\frac{1}{2}}, \quad Q = \frac{2I_{B1}}{I_{S1}}\left(\frac{I_{S2}C_1}{I_{B2}C_2}\right)^{\frac{1}{2}} \tag{9}$$

From (9), by maintaining the ratio I_{B2} and I_{S2} to be constant, it can be remarked that the pole frequency can be adjusted by I_{B2} and I_{S2} without affecting the quality factor. Moreover, the Quality factor can also be adjusted by I_{B1} or I_{S1} or both, without affecting the pole frequency. In addition, bandwidth (BW) of the system can be expressed by

$$BW = \frac{\omega_0}{Q} = \frac{1}{V_TC_1}\frac{I_{S1}I_{B2}}{I_{B1}} \tag{10}$$

Equations (9) and (10) show that the pole frequency and quality factor of the proposed filter circuit can be tuned independently and electronically with out affecting the bandwidth over the wide range by adjusting the external bias current I_{S2}.

3. Non-Ideal Analysis

For non-ideal case, the CCCCTA can be, respectively,

characterized with the following equations

$$V_{Xi} = \beta_i V_{Yi} + I_{Xi} R_{Xi} \quad (11)$$

$$I_{Zi} = \alpha_i I_{Xi} \quad (12)$$

$$I_{Oi} = \gamma_{pi} g_{mi} V_{Zi} \quad (13)$$

$$I_{-Oi} = -\gamma_{ni} g_{mi} V_{Zi} \quad (14)$$

where β_i, α_i, γ_{pi}, and γ_{ni} are transferred ratios of i^{th} CCCCTA (I = 1, 2, 3) which deviate from 'unity' by the transfer errors. In the case of non-ideal and re-analyzing the proposed filter in **Figure 3**, it yields the transfer functions as

$$T_{LP}(s) = \frac{I_{LP}(s)}{I_{in}(s)} = -g_{m1}R_{X1}\frac{\alpha_2\beta_2\gamma_{p1}\gamma_{p2}g_{m2}}{s^2\alpha_1\beta_1C_1C_2R_{X2} + s\alpha_2\beta_2\gamma_{p1}g_{m1}R_{X1}C_2 + \alpha_1\beta_1\alpha_2\beta_2\gamma_{n2}g_{m2}} \quad (15)$$

$$T_{BP}(s) = \frac{I_{BP}(s)}{I_{in}(s)} = -g_{m1}R_{X1}\frac{\frac{\beta_2\gamma_{p1}\gamma_{p3}}{(1+\alpha_3)}g_{m3}R_{X3}C_2 s}{s^2\alpha_1\beta_1C_1C_2R_{X2} + s\alpha_2\beta_2\gamma_{p1}g_{m1}R_{X1}C_2 + \alpha_1\beta_1\alpha_2\beta_2\gamma_{n2}g_{m2}} \quad (16)$$

$$T_{HP}(s) = \frac{I_{HP}(s)}{I_{in}(s)} = g_{m1}R_{X1}\frac{s^2\gamma_{n1}C_1C_2R_{X2} + \alpha_2\beta_2g_{m2}(\gamma_{n1}\gamma_{n2} - \gamma_{p1}\gamma_{p2})}{s^2\alpha_1\beta_1C_1C_2R_{X2} + s\alpha_2\beta_2\gamma_{p1}g_{m1}R_{X1}C_2 + \alpha_1\beta_1\alpha_2\beta_2\gamma_{n2}g_{m2}} \quad (17)$$

$$T_{BR}(s) = \frac{I_{BR}(s)}{I_{in}(s)} = g_{m1}R_{X1}\frac{(s^2\gamma_{n1}C_1C_2R_{X2} + \alpha_2\beta_2\gamma_{n1}\gamma_{n2}g_{m2})}{s^2\alpha_1\beta_1C_1C_2R_{X2} + s\alpha_2\beta_2\gamma_{p1}g_{m1}R_{X1}C_2 + \alpha_1\beta_1\alpha_2\beta_2\gamma_{n2}g_{m2}} \quad (18)$$

$$T_{AP}(s) = \frac{I_{AP}(s)}{I_{in}(s)} = -g_{m1}R_{X1}\frac{(s^2\gamma_{p1}C_1C_2R_{X2} - \frac{\beta_2\gamma_{p1}\gamma_{n3}}{(1+\alpha_3)}g_{m3}R_{X3}C_2 s + \alpha_2\beta_2\gamma_{p1}\gamma_{n2}g_{m2})}{s^2\alpha_1\beta_1C_1C_2R_{X2} + s\alpha_2\beta_2\gamma_{p1}g_{m1}R_{X1}C_2 + \alpha_1\beta_1\alpha_2\beta_2\gamma_{n2}g_{m2}} \quad (19)$$

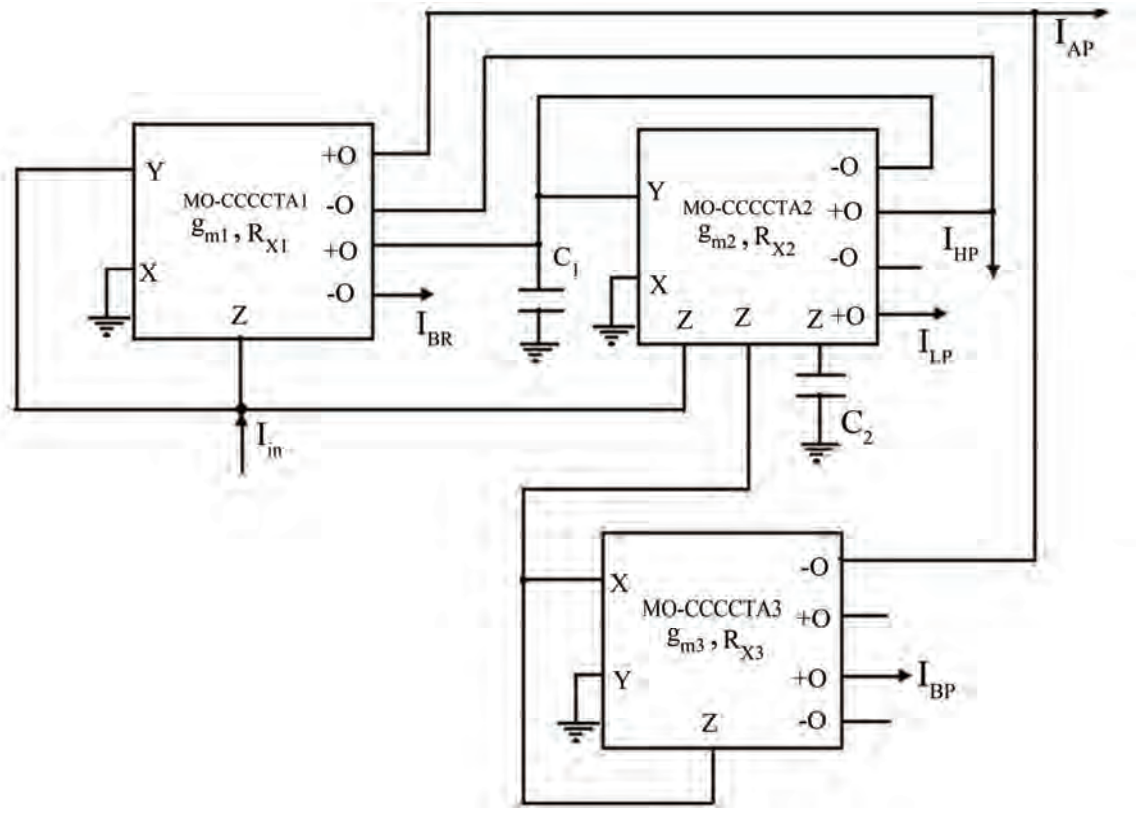

Figure 3. Proposed universal current-controlled current-mode biquad filter employing MO-CCCCTAs and grounded capacitors.

In this case, the ω_o and Q are changed to

$$\omega_o = \left(\frac{\alpha_2\gamma_{n2}\beta_2 g_{m2}}{C_1C_2R_{X2}}\right)^{\frac{1}{2}}, Q = \frac{\alpha_1\beta_1}{\gamma_{p1}g_{m1}R_{X1}}\left(\frac{\gamma_{n2}R_{X2}g_{m2}C_1}{\alpha_2\beta_2C_2}\right)^{\frac{1}{2}} \quad (20)$$

The active and passive sensitivities of the proposed circuit can be found as

$$S^{\omega_o}_{C_1,C_2,R_{X2}} = -\frac{1}{2}, S^{\omega_o}_{g_{m2},\alpha_2,\beta_2,\gamma_{n2}} = \frac{1}{2}, S^{\omega_o}_{R_{X1},g_{m1},g_{m3},\alpha_1,\alpha_3,\beta_1,\beta_3} = 0,$$
$$S^{\omega_o}_{R_{X3},\gamma_{n1},\gamma_{n3},\gamma_{p1},\gamma_{p2},\gamma_{p3}} = 0 \quad (21)$$

$$S^{Q}_{C_2,\alpha_2,\beta_2} = -\frac{1}{2}, \quad S^{Q}_{R_{X2},g_{m2},C_1,\gamma_{n2}} = \frac{1}{2}, \quad S^{Q}_{\gamma_{p1},g_{m1},R_{X1}} = -1,$$
$$S^{Q}_{\alpha_1,\beta_1} = 1 \quad S^{Q}_{\alpha_3,\gamma_{n1},\gamma_{n3},\gamma_{p2},\gamma_{p3},\beta_3,g_{m3}} = 0 \quad (22)$$

From the above results, it can be observed that all the sensitivities are low and no longer than one in magnitude.

4. Simulation Results

The proposed universal current-mode filter was verified through PSPICE simulations. In simulation, the MO-CCCCTA was realized using BJT model as shown in **Figure 2**, with the transistor model of HFA3096 mixed transistors arrays [12] and was biased with ±1.85 V DC power supplies. The SPICE model parameters are given in **Table 1**. The circuit was designed for Q = 1 and f_o = $\omega_o/2\pi$ = 3.68 MHz. The active and passive components were chosen as I_{B1} = I_{B2} = 60 μA, I_{B3} = 30 μA I_{S1} = I_{S2} = I_{S3} = 240 μA and C_1 = C_2 = 0.2 nF. **Figure 4** shows the simulated gain responses of the *LP*, *HP*, *BP*, *BR* and *AP* in current form. **Figure 5** shows the phase response of *AP*. The simulation results show the simulated pole frequency as 3.58 MHz that agree quite well with the theoretical analysis.

Figure 6 shows magnitude responses of BP function where I_{B2} and I_{S2} are equally set and changed for several values, by keeping its ratio to be constant for constant Q(= 2). Other parameters were chosen as I_{B1} = 240 μA, I_{B3} = 30 μA, I_{S1} = I_{S3} = 240 μA, and C_1 = C_2 = 0.2 nF. The pole frequency (in **Figure 6**) is found to vary as 1.75 MHz, 3.43 MHz and 7.52 MHz for three values of I_{B2} = I_{S2} as 60 μA, 120 μA and 280 μA, respectively, which shows that pole frequency can be electronically adjusted without affecting the quality factor. **Figure 7** shows the magnitude responses of BP function for different values of $I_{S1,}$ by keeping I_{B1} = I_{B2} = 60 μA, I_{B3} = 30 μA, I_{S2} = I_{S3} = 240 μA, and C_1 = C_2 = 0.2 nf. The quality factor was found to vary as 7.2, 3.81, 1.91, 0.96, 0.49, by keeping constant pole frequency as 3.35 MHz for five values of I_{S1} as 30 μA, 60 μA, 120 μA, 240 μA and 480 μA, respectively, which shows that the quality factor of the BP response can be electronically adjusted without affecting the pole frequency by input bias current I_{S1}. Further simulations were carried out to verify the total harmonic

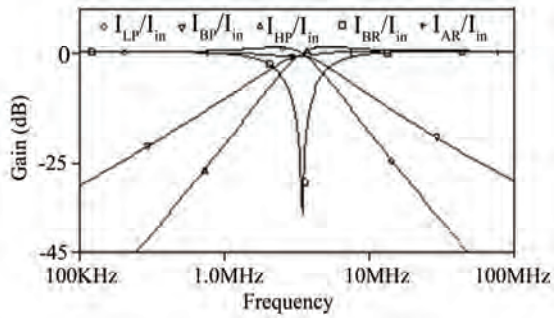

Figure 4. Simulated results of circuit in Figure 3.

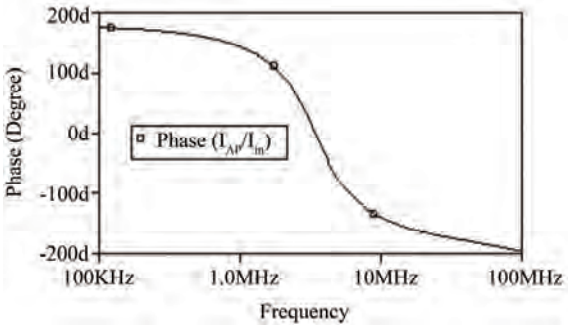

Figure 5. Phase response of AP of circuit in Figure 3.

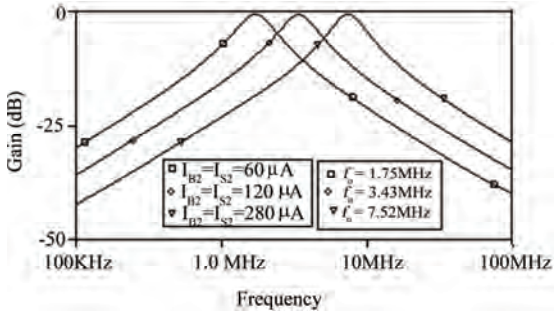

Figure 6. Band Pass responses for different value of I_{B2} = I_{S2}.

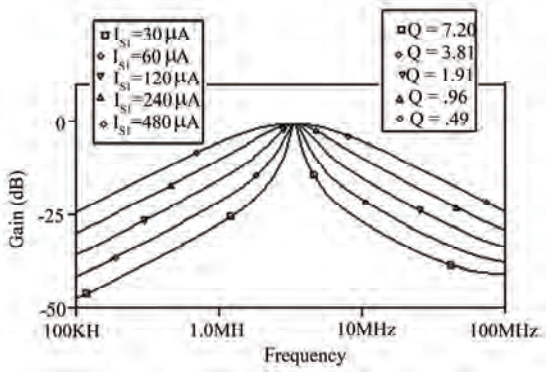

Figure 7. Band Pass responses for different value of I_{S1}.

Table 1. The SPICE model parameters of HFA3096 mixed transistors arrays.

.model npn	Is = 1.80E − 17, Xti = 3.20, Eg = 1.167, Vaf = 151.0, Bf = 1.10E + 02, Ne = 2.000, Ise = 1.03E − 16, IKf = 1.18E − 02, Xtb = 2.15, Br = 8.56E − 02, IKr = 1.18E − 02, Rc = 1.58E + 02, Cjc = 2.44E − 14, Mjc = 0.350, Vjc = 0.633, Cje = 5.27E − 4,Mje = 0.350, Vje = 1.250, Tr = 5.16E − 08, Tf = 2.01E − 11, Itf = 2.47E − 02, Vtf = 6.62, Xtf = 25.98, Rb = 8.11E + 02, Ne = 2, Isc = 0, Fc = .5
.model pnp	Is = 8.40E − 18, Xti = 3.67, Eg = 1.145, Vaf = 57.0, Bf = 9.55E + 01, Ne = 2.206, Ise = 3.95E − 16, IKf = 2.21E − 03, Xtb = 1.82, Br = 3.40E − 01, IKr = 2.21E − 03, Rc = 1.43E + 02, Cjc = 3.68E − 14, Mjc = 0.333, Vjc = 0.700, Cje = 4.20E − 14, Mje = 0.560, Vje = .8950, Tr = 2.10E − 08, Tf = 6.98E − 11, Itf = 2.25E − 02, Vtf = 1.34, Xtf = 12.31, Rb = 5.06E + 02, Ne = 2, Isc = 0, Fc = .5

distortion (THD). The circuit was verified by applying a sinusoidal input current of varying frequency and amplitude of 60 μA. The THD measured at the LP output are found to be less than 3% while frequency is varied from 30 KHz to 1 MHz. Moreover, the circuit was also simulated for THD analysis at LP output, by applying sinusoidal input current of varying amplitude and constant frequency. **Figure 8** shows the variation of THD versus applied sinusoidal input current at frequency of 500 KHz for the proposed filter. It can be seen that the THD of the proposed filter circuit for the input current signal less than 100 μA, remain in moderate range, *i.e*., 3%. The time domain response of current-mode *LP* output (I_{LP}) is shown in **Figure 9**. It was observed that 120 μA peak to peak input current sinusoidal signal levels having frequency 500 KHz are possible without significant distortions. Thus both THD analysis and time domain response of LP output confirm the practical utility of the proposed current-mode filter circuit.

5. Conclusions

A new universal current-controlled current-mode biquad filter employing three MO-CCCCTAs and two grounded capacitors is proposed. The proposed filter offers the following advantages: 1) employment of only three active elements; 2) ability of realizing all current-mode standard filter functions simultaneously; 3) employment of Both grounded capacitors; 4) low sensitivity figures and low THD; 5) electronically orthogonal tunability of ω_o and Q; 6) availability of explicit current outputs (*i.e.*, high impedance output nodes) without requiring any additional active elements; 7) suitable for high frequency applications - all of which are not available simultaneously in any of the previously reported current-controlled current-mode biquad filter of [6,8,10,12-19,21-23]. With above mentioned features it is very suitable to realize the proposed circuit in monolithic chip to use in battery powered, portable electronic equipments such as wireless communication system devices.

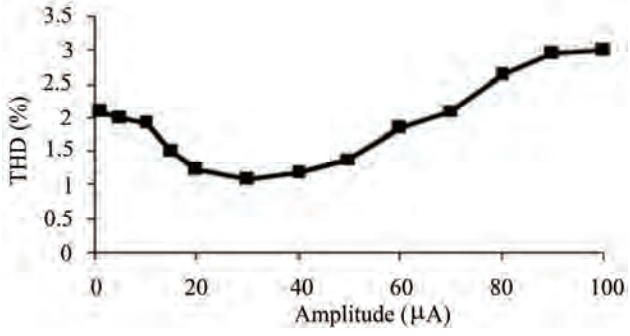

Figure 8. Variation of THD of LP output with input current signal at 500 KHz.

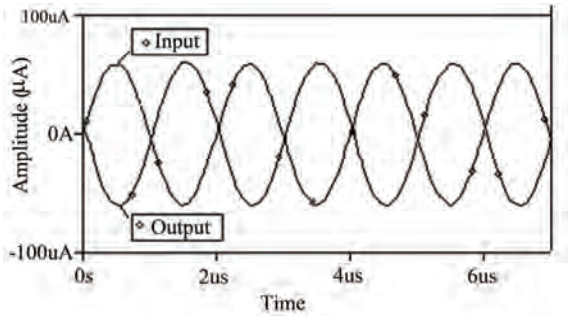

Figure 9. The time domain input waveform and corresponding response at LP output.

6. References

[1] A. S. Sedra and K. C. Smith, "Microelectronics Circuits," Rinehart and Winston, Holt, 2003.

[2] C. Toumazou, F. J. Lidgey and D. G. Haigh, "Analogue IC Design: The Current-Mode Approach," London Peter Peregrinus, London, 1990.

[3] M. Siripruchyanun and W. Jaikla, "Current Controlled Current Conveyor Transconductance Amplifier (CCCCTA): A Building Block for Analog Signal Processing," *Electrical Engineering*, Vol. 90, No. 6, 2008, pp. 443-453.

[4] S. V. Singh, S. Maheshwari, J. Mohan and D. S. Chauhan, "An Electronically Tunable SIMO Biquad Filter Using CCCCTA," *Contemporary Computing*, *CCIS*, Vol. 40,

2009, pp. 544-555.

[5] A. M. Soliman, "New Current-Mode Filters Using Current Conveyors," *International Journal of Electronics and Communications* (*AEÜ*), Vol. 51, No. 3, 1997, pp. 275-278.

[6] S. Minaei and S. Türköz, "New Current-Mode Current-Controlled Universal Filter with Single Input and Three Outputs," *International Journal of Electronics*, Vol. 88, No. 3, 2001, pp. 333-337.

[7] R. Senani, "New Current Mode Biquad Filter," *International Journal of Electronics*, Vol. 73, No. 4, 1992, pp. 735-742.

[8] A. U. Keskin, D. Biolek, E. Hancioglu and V. Biolkova, "Current-Mode KHN Filter Employing Current Differencing Transconductance Amplifiers," *International Journal of Electronics and Communications* (*AEÜ*), Vol. 60, No. 6, 2006, pp. 443-446.

[9] M. Soliman, "Current Mode Universal Filters with Grounded Passive Elements and Using Single Output Current Conveyors," *Journal of Active and Passive Electronics Devices*, Vol. 4, 2009, pp. 55-62.

[10] S. Maheshwari and I. A. Khan, "Novel Cascadable Current-Mode Translinear-C Universal Filter," *Active Passive Electronics Components*, Vol. 27, No. 4, 2004, pp. 215-218.

[11] C. Wang, Y. Zhao, Q. Zhang and S. Du, "A New Current Mode SIMO-Type Universal Biquad Employing Multi-Output Current Conveyors (MOCCIIs)," *Radioengineering*, Vol. 18, No. 1, 2009, pp. 83-88.

[12] R. Senani, V. K. Singh, A. K. Singh and D. R. Bhaskar, "Novel Electronically Controllable Current-Mode Universal Biquad Filter," *The Institute of Electronics, Information and Communication Engineers*, Vol. 1, No. 14, 2004, pp. 410-415.

[13] W. Kiranon, J. Kesorn and N. Kamprasert, "Electronically Tunable Multi-Function Translinear-C Filter and Oscillators," *Electronics Letters*, Vol. 33, No. 7, 1997, pp. 573-574.

[14] S. Maheshwari and I. A. Khan, "High Performance Versatile Translinear-C Universal Filter," *Journal of Active and Passive Electronics Devices*, Vol. 1, No. 2, 2005, pp. 41-51.

[15] M. T. Abuelma'atti and N. A. Tassaduq, "New Current-Mode Current Controlled Filters Using Current-Controlled Conveyor," *International Journal of Electronics*, Vol. 85, No. 4, 1998, pp. 483-488.

[16] T. Katoh, T. Tsukutani, Y. Sumi and Y. Fukui, "Electronically Tunable Current-Mode Universal Filter Employing CCCIIs and Grounded Capacitors," *International Symposium on Intelligent Signal Processing and Communications Systems*, 2006, pp. 107-110.

[17] C. Wang, H. Liu and Y. Zhao, "A New Current-Mode Current-Controlled Universal Filter Based on CCCII (±)," *Circuits System Signal Processing*, Vol. 27, No. 5, 2008, pp. 673-682.

[18] S. Minaei and S. Türköz, "Current-Mode Electronically Tunable Universal Filter Using Only Plus-Type Current Controlled Conveyors and Grounded Capacitors," *Electronics and Telecommunications Research Institute Journal*, Vol. 26, No. 4, 2004, pp. 292-296.

[19] M. T. Abuelma'atti and N. A. Tassaduq, "A Novel Single-Input Multiple-Output Current-Controlled Universal Filter," *Microelectronics Journal*, Vol. 29, No. 11, 1998, pp. 901-905.

[20] S. Maheshwari, "Current-Mode Filters with High Output Impedance and Employing only Grounded Components," *WSEAS Transactions on Electronics*, Vol. 5, No. 1, 2008, pp. 238-243.

[21] W. Jaikla and M. Siripruchyanun, "A Cascadable Current-Mode Universal Biquadratic Filter Using MO-CCCCTAs," *IEEE Conference*, Pisa, 2008, pp. 952-955.

[22] D. Biolek and V. Biolkova, "CDTA-C Current-Mode Universal 2nd Order Filter," *Proceeding of the 5th International Conference on Applied Informatics and Communications*, Malta, 2003, pp. 411-414.

[23] W. Tangsrirat and W. Surakampontorn, "Systematic of Cascadable Current-Mode Filters Using CDTAs," *Frequenz*, Vol. 60, No. 11-12, 2006, pp. 241-245.

Circuits and Systems, **2010, 1, 41-48**
doi:10.4236/cs.2010.12007 Published Online October 2010 (http://www.SciRP.org/journal/cs)

Decoupling Zeros of Positive Discrete-Time Linear Systems*

Tadeusz Kaczorek
Faculty of Electrical Engineering, Bialystok University of Technology, Bialystok, Poland
E-mail: *kaczorek@isep.pw.edu.pl*
Received July 13, 2010; *revised August* 16, 2010; *accepted August* 20, 2010

Abstract

The notions of decoupling zeros of positive discrete-time linear systems are introduced. The relationships between the decoupling zeros of standard and positive discrete-time linear systems are analyzed. It is shown that: 1) if the positive system has decoupling zeros then the corresponding standard system has also decoupling zeros, 2) the positive system may not have decoupling zeros when the corresponding standard system has decoupling zeros, 3) the positive and standard systems have the same decoupling zeros if the rank of reachability (observability) matrix is equal to the number of linearly independent monomial columns (rows) and some additional assumptions are satisfied.

Keywords: Input-Decoupling Zeros, Output-Decoupling Zeros, Input-Output Decoupling Zeros, Positive, Discrete-Time, Linear, System

1. Introduction

In positive systems inputs, state variables and outputs take only non-negative values. Examples of positive systems are industrial processes involving chemical reactors, heat exchangers and distillation columns, storage systems, compartmental systems, water and atmospheric pollution models. A variety of models having positive linear behavior can be found in engineering, management science, economics, social sciences, biology and medicine, etc. An overview of state of the art in positive linear theory is given in the monographs [1,2].

The notions of controllability and observability and the decomposition of linear systems have been introduced by Kalman [3,4]. Those notions are the basic concepts of the modern control theory [5-9]. They have been also extended to positive linear systems [1,2].

The reachability and controllability to zero of standard and positive fractional discrete-time linear systems have been investigated in [10]. The decomposition of positive discrete-time linear systems has been addressed in [11]. The notion of decoupling zeros of standard linear systems have been introduced by Rosebrock [8,12].

In this paper the notions of decoupling zeros will be extended for positive discrete-time linear systems.

The paper is organized as follows. In Section 2 the basic definitions and theorems concerning reachability and observability of positive discrete-time linear systems are recalled. The decomposition of the pair (A,B) and (A,C) of positive linear system is addressed in Section 3. The main result of the paper is given in Section 4 where the definitions of the decoupling-zeros are proposed and the relationships between decoupling zeros of standard and positive discrete-time linear systems are discussed. Concluding remarks are given in Section 5.

*This work was supported by Ministry of Science and Higher Education in Poland under work No NN514 1939 33.

2. Preliminaries

The set of $n \times m$ real matrices will be denoted by $\Re^{n \times m}$ and $\Re^n := \Re^{n \times 1}$. The set of $m \times n$ real matrices with nonnegative entries will be denoted by $\Re_+^{m \times n}$ and $\Re_+^n := \Re_+^{n \times 1}$. The set of nonnegative integers will be denoted by Z_+ and the $n \times n$ identity matrix by I_n.

Consider the linear discrete-time systems

$$\begin{aligned} x_{i+1} &= Ax_i + Bu_i, \quad i \in Z_+ \\ y_i &= Cx_i + Du_i \end{aligned} \tag{2.1}$$

where $x_i \in \Re^n$, $u_i \in \Re^m$, $y_i \in \Re^p$ are the state, input and output vectors and $A \in \Re^{n \times n}$, $B \in \Re^{n \times m}$, $C \in \Re^{p \times n}$, $D \in \Re^{p \times m}$.

Definition 2.1. The system (2.1) is called (internally) positive if and only if $x_i \in \Re_+^n$, and $y_i \in \Re_+^p$, $i \in Z_+$ for every $x_0 \in \Re_+^n$, and any input sequence $u_i \in \Re_+^m$, $i \in Z_+$.

Theorem 2.1. [1,2] The system (2.1) is (internally) positive if and only if

$A \in \Re_+^{n\times n}$, $B \in \Re_+^{n\times m}$, $C \in \Re_+^{p\times n}$, $D \in \Re_+^{p\times m}$. (2.2)

Definition 2.2. The positive system (2.1) is called reachable in q steps if there exists an input sequence $u_i \in \Re_+^m$, $i = 0,1,...,q-1$ which steers the state of the system from zero ($x_0 = 0$) to any given final state $x_f \in \Re_+^n$, *i.e.*, $x_f = x_0$.

Let e_i, i = 1,…,n be the ith column of the identity matrix I_n. A column ae_i for $a > 0$ is called the monomial column.

Theorem 2.2. [1,2] The positive system (2.1) is reachable in q steps if and only if the reachability matrix

$$R_q = [B \quad AB \quad ... \quad A^{q-1}B] \in \Re_+^{n\times qm} \tag{2.3}$$

contains n linearly independent monomial columns.

Theorem 2.3. [1,2] The positive system (2.1) is reachable in q steps only if the matrix

$$[B \quad A] \tag{2.4}$$

contains n linearly independent monomial columns.

Definition 2.3. The positive systems (2.1) is called observable in q steps if it is possible to find unique initial state $x_0 \in \Re_+^n$ of the system knowing its input sequence $u_i \in \Re_+^m$, $i = 0,1,...,q-1$ and its corresponding output sequence $y_i \in \Re_+^p$, $i = 0,1,...,q-1$.

Theorem 2.4. [1,2] The positive systems (2.1) is observable in q steps if and only if the observability matrix

$$O_q = \begin{bmatrix} C \\ CA \\ \vdots \\ CA^{q-1} \end{bmatrix} \in \Re_+^{qp\times n} \tag{2.5}$$

contains n linearly independent monomial rows.

Theorem 2.5. [1,2] The positive system (2.1) is observable in q steps only if the matrix

$$\begin{bmatrix} C \\ A \end{bmatrix} \tag{2.6}$$

contains n linearly independent monomial rows.

3. Decomposition of Positive Pair (*A*,*B*) and (*A*,*C*) of Positive Linear Systems

Let the reachability matrix

$$R_n = [B \quad AB \quad ... \quad A^{n-1}B] \in \Re_+^{n\times mn} \tag{3.1}$$

of the positive system (2.1) has $n_1 < n$ linearly independent monomial columns and let the columns

$$B_{i_1}, B_{i_2}, ..., B_{i_k} \quad (k \le m) \tag{3.2}$$

of the matrix $B \in \Re_+^{n\times m}$ be linearly independent monomial columns. We choose from the sequence

$$AB_{i_1}, ..., AB_{i_k}, A^2B_{i_1}, ..., A^2B_{i_k}, ..., A^{n-1}B_{i_1}, ..., A^{n-1}B_{i_k} \tag{3.3}$$

monomial columns which are linearly independent from (3.2) and previously chosen monomial columns. From those monomial columns we build the monomial matrix

$$\begin{aligned} P &= [P_{i_1} \quad ... \quad P_{i_1 d_1} \quad P_{i_2} \quad ... \quad P_{i_2 d_2} \quad ... \quad P_{i_k d_k} \quad P_{n_1+1} \quad ... \quad P_n] \\ &= [P_1 \quad P_2 \quad ... \quad P_n] \end{aligned} \tag{3.4a}$$

where

$$\begin{aligned} &P_{i_1} = B_{i_1}, ..., P_{i_1 d_1} = A^{d_1-1}B_{i_1}, \\ &P_{i_2} = B_{i_2}, ..., P_{i_2 d_2} = A^{d_2-1}B_{i_2}, ..., P_{i_k d_k} = A^{d_k-1}B_{i_k} \end{aligned} \tag{3.4b}$$

and d_i $(i = 1,...,k)$ are some natural numbers.

Theorem 3.1. Let the positive system (2.1) be unreachable, the reachability matrix (3.1) have $n_1 < n$ linearly independent monomial columns and the assumption

$$P_k^T A P_j = 0 \quad \text{for} \quad k = n_1+1, ..., n; \quad j = 1, ..., n_1 \tag{3.5}$$

be satisfied.

Then the pair (A, B) of the system can be reduced by the use of the matrix (3.4) to the form

$$\begin{aligned} &\bar{A} = P^{-1}AP = \begin{bmatrix} \bar{A}_1 & \bar{A}_{12} \\ 0 & \bar{A}_2 \end{bmatrix}, \quad \bar{B} = P^{-1}B = \begin{bmatrix} \bar{B}_1 \\ 0 \end{bmatrix}, \\ &\bar{A}_1 \in \Re_+^{n_1\times n_1}, \quad \bar{A}_2 \in \Re_+^{n_2\times n_2}, \quad (n_2 = n - n_1) \\ &\bar{A}_{12} \in \Re_+^{n_1\times n_2}, \quad \bar{B}_1 \in \Re_+^{n_1\times m} \end{aligned} \tag{3.6}$$

where the pair $(\bar{A}_1, \bar{B}_1)$ is reachable and the pair $(\bar{A}_2, \bar{B}_2 = 0)$ is unreachable.

Proof is given in [11].

Theorem 3.2. The transfer matrix

$$T(z) = C[I_n z - A]^{-1}B + D \tag{3.7}$$

of the positive system (2.1) is equal to the transfer matrix

$$T_1(z) = \bar{C}_1[I_{n_1} z - \bar{A}_1]^{-1}\bar{B}_1 + D \tag{3.8}$$

of its reachable part $(\bar{A}_1, \bar{B}_1, \bar{C}_1)$, where $CP = [\bar{C}_1 \quad \bar{C}_2]$, $\bar{C}_1 \in \Re_+^{p\times n_1}$.

Proof is given in [11].

By duality principle [11] we can obtained similar (dual) result for the pair (*A*,*C*) of the positive system (2.1).

Let the observability matrix

$$O_n = \begin{bmatrix} C \\ CA \\ \vdots \\ CA^{n-1} \end{bmatrix} \in \Re_+^{qn\times n} \tag{3.9}$$

has $n_1 < n$ linearly independent monomial rows.

In a similar way as for the pair (*A*,*B*) by the choice of n_1 linearly independent monomial row for the pair (*A*,*C*) we may find the monomial matrix $Q \in \Re_+^{n\times n}$ of the form [11]

$$Q^T = [Q_{j_1}^T \quad ... \quad Q_{j_1\bar{d}_1}^T \quad Q_{j_2}^T \quad ... \quad Q_{j_2\bar{d}_2}^T \quad ... \quad Q_{j_l\bar{d}_l}^T \quad Q_{n_1+1}^T \quad ... \quad Q_n^T] \tag{3.10a}$$

where

$$Q_{j_1} = C_{j_1}, ..., Q_{j_1\bar{d}_1} = C_{j_1} A^{\bar{d}_1 - 1},$$
$$Q_{j_2} = C_{j_2}, ..., Q_{j_2\bar{d}_2} = C_{j_2} A^{\bar{d}_2 - 1}, ..., Q_{j_l\bar{d}_l} = C_{j_l} A^{\bar{d}_l - 1} \quad (3.10b)$$

and $\bar{d}_j$ $(j = 1, ..., l)$ are some natural numbers.

Theorem 3.3. Let the positive system (2.1) be unobservable, the matrix (3.9) has $n_1 < n$ linearly independent monomial rows and the assumption

$$Q_k A Q_j^T = 0 \quad \text{for} \quad k = 1, ..., n_1; \quad j = n_1 + 1, ..., n \quad (3.11)$$

be satisfied.

Then the pair (A,C) of the system can be reduced by the use of the matrix (3.10) to the form

$$\hat{A} = QAQ^{-1} = \begin{bmatrix} \hat{A}_1 & 0 \\ \hat{A}_{21} & \hat{A}_2 \end{bmatrix}, \quad \hat{C} = CQ^{-1} = [\hat{C}_1 \quad 0]$$
$$\hat{A}_1 \in \Re_+^{n_1 \times n_1}, \quad \hat{A}_2 \in \Re_+^{n_2 \times n_2}, \quad (n_2 = n - n_1) \quad (3.12)$$
$$\hat{A}_{21} \in \Re_+^{n_2 \times n_1}, \quad \hat{C}_1 \in \Re_+^{p \times n_1}$$

where the pair $(\hat{A}_1, \hat{C}_1)$ is observable and the pair $(\hat{A}_2, \hat{C}_2 = 0)$ is unobservable.

Proof is given in [11].

Theorem 3.4. The transfer matrix (3.7) of the positive system (2.1) is equal to the transfer matrix

$$T_1(z) = \hat{C}_1 [I_{n_1} z - \hat{A}_1]^{-1} \hat{B}_1 + D \quad (3.13)$$

where

$$QB = \begin{bmatrix} \hat{B}_1 \\ \hat{B}_2 \end{bmatrix}, \quad \hat{B}_1 \in \Re^{n_1 \times m}, \quad \hat{B}_2 \in \Re^{n_2 \times m}. \quad (3.14)$$

Proof is given in [11].

Remark 3.1. From Theorem 3.1 and 3.3 it follows that the conditions for decomposition of the pair (A,B) and (A,C) of the positive system (2.1) are much stronger than of the pairs of the standard system.

4. Decoupling Zeros of the Positive Systems

It is well-known [5-8] that the input-decupling zeros of standard linear systems are the eigenvalues of the matrix A_2 of the unreachable (uncontrollable) part of the system. Similarly, the output-decoupling zeros of standard linear systems are the eigenvalues of the matrix of the unreachable and unobservable parts of the system. In a similar way we will defined the decoupling zeros of the positive linear discrete-time systems.

Definition 4.1. Let $\bar{A}_2 \in \Re_+^{\bar{n}_2 \times \bar{n}_2}$ be the matrix of unreachable part of the system (2.1). The zeros $z_{i1}, z_{i2}, ..., z_{i\bar{n}_2}$ of the characteristic polynomial

$$\det[I_{\bar{n}_2} z - \bar{A}_2] = z^{\bar{n}_2} + \bar{a}_{\bar{n}_2 - 1} z^{\bar{n}_2 - 1} + ... + \bar{a}_1 z + \bar{a}_0 \quad (4.1)$$

of the matrix $\bar{A}_2$ are called the input-decoupling zero of the positive system (2.1).

The list of the input-decoupling zeros will be denoted by $Z_i = \{z_{i1}, z_{i2}, ..., z_{i\bar{n}_2}\}$.

Example 4.1. Consider the positive system (2.1) with the matrices

$$A = \begin{bmatrix} 1 & 0 & 2 \\ 0 & 2 & 0 \\ 0 & 0 & 3 \end{bmatrix}, \quad B = \begin{bmatrix} 1 \\ 0 \\ 0 \end{bmatrix} \quad (4.2)$$

Note that the pair (4.2) has already the form (3.6) with

$$\bar{A} = A = \begin{bmatrix} \bar{A}_1 & \bar{A}_{12} \\ 0 & \bar{A}_2 \end{bmatrix} = \begin{bmatrix} 1 & 0 & 2 \\ 0 & 2 & 0 \\ 0 & 0 & 3 \end{bmatrix},$$
$$\bar{B} = B = \begin{bmatrix} \bar{B}_1 \\ 0 \end{bmatrix} = \begin{bmatrix} 1 \\ 0 \\ 0 \end{bmatrix}, \quad (n_1 = 1, n_2 = 2) \quad (4.3)$$

In this case the characteristic polynomial of the matrix $\bar{A}_2 = \begin{bmatrix} 2 & 0 \\ 0 & 3 \end{bmatrix}$ has the form

$$\det[I_2 z - \bar{A}_2] = \begin{vmatrix} z-2 & 0 \\ 0 & z-3 \end{vmatrix}, \quad (4.4)$$
$$= (z-2)(z-3) = z^2 - 5z + 6$$

the input-decoupling zeros are equal to $z_{i1} = 2, z_{i2} = 3$ and $Z_i = \{2, 3\}$.

Definition 4.2. Let $\hat{A}_2 \in \Re_+^{\hat{n}_2 \times \hat{n}_2}$ be the matrix of unobservable part of the system (2.1). The zeros $z_{o1}, z_{o2}, ..., z_{o\bar{n}_2}$ of the characteristic polynomial

$$\det[I_{\hat{n}_2} z - \hat{A}_2] = z^{\hat{n}_2} + \hat{a}_{\hat{n}_2 - 1} z^{\hat{n}_2 - 1} + ... + \hat{a}_1 z + \hat{a}_0 \quad (4.5)$$

of the matrix $\hat{A}_2$ are called the output-decoupling zero of the positive system (2.1).

The list of the output-decoupling zeros will be denoted by $Z_o = \{z_{o1}, z_{o2}, ..., z_{o\hat{n}_2}\}$.

Example 4.2. Consider the positive system (2.1) with the matrices (4.2) and

$$C = [0 \quad 1 \quad 0], \quad D = [0]. \quad (4.6)$$

The observability matrix

$$O_3 = \begin{bmatrix} C \\ CA \\ CA^2 \end{bmatrix} = \begin{bmatrix} 0 & 1 & 0 \\ 0 & 2 & 0 \\ 0 & 4 & 0 \end{bmatrix} \quad (4.7)$$

has only one monomial row $Q_1 = [0 \quad 1 \quad 0]$. In this case the monomial matrix (3.10) has the form

$$Q = \begin{bmatrix} Q_1 \\ Q_2 \\ Q_3 \end{bmatrix} = \begin{bmatrix} 0 & 1 & 0 \\ 1 & 0 & 0 \\ 0 & 0 & 1 \end{bmatrix} \quad (4.8)$$

and the assumption (3.11) is satisfied since

$$Q_1 A[Q_2^T \quad Q_3^T] = [0 \quad 1 \quad 0]\begin{bmatrix}1 & 0 & 2\\ 0 & 2 & 0\\ 0 & 0 & 3\end{bmatrix}\begin{bmatrix}1 & 0\\ 0 & 0\\ 0 & 1\end{bmatrix} = [0 \quad 0] \tag{4.9}$$

Using (3.12) and (4.8) we obtain

$$\hat{A} = QAQ^{-1} = \begin{bmatrix}0 & 1 & 0\\ 1 & 0 & 0\\ 0 & 0 & 1\end{bmatrix}\begin{bmatrix}1 & 0 & 2\\ 0 & 2 & 0\\ 0 & 0 & 3\end{bmatrix}\begin{bmatrix}0 & 1 & 0\\ 1 & 0 & 0\\ 0 & 0 & 1\end{bmatrix}$$

$$= \begin{bmatrix}2 & 0 & 0\\ 0 & 1 & 2\\ 0 & 0 & 3\end{bmatrix} = \begin{bmatrix}\hat{A}_1 & 0\\ \hat{A}_{21} & \hat{A}_2\end{bmatrix}, \quad (n_1 = 1, n_2 = 2)$$

$$\hat{C} = CQ^{-1} = [\hat{C}_1 \quad 0] = [1 \quad 0 \quad 0]$$

Characteristic polynomial of the matrix $\hat{A}_2 = \begin{bmatrix}1 & 2\\ 0 & 3\end{bmatrix}$ has the form

$$\det[I_2 z - \hat{A}_2] = \begin{vmatrix}z-1 & -2\\ 0 & z-3\end{vmatrix} = (z-1)(z-3) = z^2 - 4z + 3$$

the output-decoupling zeros are equal to $z_{o1} = 1, z_{o2} = 3$ and $Z_o = \{1,3\}$.

Definition 4.3. Zeros $z_{i0}^{(1)}, z_{i0}^{(2)}, ..., z_{i0}^{(k)}$ which are simultaneously the input-decoupling zeros and the output-decoupling zeros of the positive system (2.1) are called the input-output decoupling zeros of the positive system, *i.e.*,

$$z_{i0}^{(j)} \in Z_i \quad \text{and} \quad z_{i0}^{(j)} \in Z_o \quad \text{for } j = 1,\ldots,k; \quad k \le \min(\bar{n}_2, \hat{n}_2) \tag{4.10}$$

The list of input-output decoupling zeros will be denoted by $Z_{i0} = \{z_{i0}^{(1)}, z_{i0}^{(2)}, ..., z_{i0}^{(k)}\}$.

Example 4.3. Consider the positive system (2.1) with the matrices (4.2) and (4.6). The system has the input-decoupling $z_{i1} = 2, z_{i2} = 3$ and $Z_i = \{2,3\}$ (Example 4.1) and the output-decoupling zero $z_{o1} = 1, z_{o2} = 3$ and $Z_o = \{1,3\}$ (Example 4.2). Therefore, by Definition 4.3 the positive system has one input-output decoupling zero $z_{io} = 3$, $Z_{io} = \{3\}$. This zero is the eigenvalue of the matrix $A_{12} = [3]$ of the unreachable and unobservable part of the system. Note that the transfer function of the system is zero, *i.e.*,

$$T(s) = C[I_n z - A]^{-1} B + D$$

$$= \begin{bmatrix}0 & 1 & 0\end{bmatrix}\begin{bmatrix}z-1 & 0 & -2\\ 0 & z-2 & 0\\ 0 & 0 & z-3\end{bmatrix}^{-1}\begin{bmatrix}1\\ 0\\ 0\end{bmatrix} + [0] = [0] \tag{4.11}$$

since it represents the reachable and observable part of the system.

Example 4.4. Consider the positive system (2.1) with the matrices

$$A = \begin{bmatrix}1 & 0 & 2\\ 0 & 2 & 1\\ 0 & 0 & 3\end{bmatrix}, \quad B = \begin{bmatrix}1\\ 0\\ 0\end{bmatrix}, \quad C = [0 \quad 1 \quad 0], \quad D = [0]. \tag{4.12}$$

Note that the matrices *B*, *C*, *D* are the same as in Example 4.1 and 4.2 and the matrix *A* differs by only one entry $a_{23} = 1$.

The pair (*A*,*B*) has already the form (3.6) since

$$\bar{A} = A = \begin{bmatrix}\bar{A}_1 & \bar{A}_{12}\\ 0 & \bar{A}_2\end{bmatrix} = \begin{bmatrix}1 & 0 & 2\\ 0 & 2 & 1\\ 0 & 0 & 3\end{bmatrix},$$

$$\bar{B} = B = \begin{bmatrix}\bar{B}_1\\ 0\end{bmatrix} = \begin{bmatrix}1\\ 0\\ 0\end{bmatrix}, \quad (n_1 = 1, n_2 = 2) \tag{4.13}$$

The observability matrix

$$O_3 = \begin{bmatrix}C\\ CA\\ CA^2\end{bmatrix} = \begin{bmatrix}0 & 1 & 0\\ 0 & 2 & 1\\ 0 & 4 & 5\end{bmatrix} \tag{4.14}$$

has only one monomial row $Q_1 = [0 \quad 1 \quad 0]$ and

$$Q = \begin{bmatrix}0 & 1 & 0\\ 1 & 0 & 0\\ 0 & 0 & 1\end{bmatrix} \tag{4.15}$$

is the same as in Example 4.2. The positive pair (*A*,*C*) can not be decomposed because the assumption (3.11) is not satisfied, *i.e.*,

$$Q_1 A[Q_2^T Q_3^T] = [0 \quad 1 \quad 0]\begin{bmatrix}1 & 0 & 2\\ 0 & 2 & 1\\ 0 & 0 & 3\end{bmatrix}\begin{bmatrix}1 & 0\\ 0 & 0\\ 0 & 1\end{bmatrix} \tag{4.16}$$

$$= [0 \quad 1] \neq [0 \quad 0]$$

Now let us consider the standard system (2.1) with (4.12). In this case the matrix (4.14) has two linearly independent rows and

$$Q = \begin{bmatrix}0 & 1 & 0\\ 0 & 2 & 1\\ 1 & 0 & 0\end{bmatrix} \tag{4.17}$$

Using (3.12) and (4.17) we obtain

$$\hat{A} = QAQ^{-1} = \begin{bmatrix}0 & 1 & 0\\ 0 & 2 & 1\\ 1 & 0 & 0\end{bmatrix}\begin{bmatrix}1 & 0 & 2\\ 0 & 2 & 1\\ 0 & 0 & 3\end{bmatrix}\begin{bmatrix}0 & 0 & 1\\ 1 & 0 & 0\\ -2 & 1 & 0\end{bmatrix} \tag{4.18a}$$

$$= \begin{bmatrix}0 & 1 & 0\\ -6 & 5 & 0\\ -4 & 2 & 1\end{bmatrix} = \begin{bmatrix}\hat{A}_1 & 0\\ \hat{A}_{21} & \hat{A}_2\end{bmatrix}$$

and

$$\hat{C} = CQ^{-1} = [\hat{C}_1 \quad 0] = [1 \quad 0 \quad 0], \ (n_2 = n - n_1) \quad (4.18b)$$

The matrix $\hat{A}_2 = [1]$ of the unobservable part of the standard system has one eigenvalue which is equal to the output-decoupling zero $z_{o1} = 1$. Note that the standard system has two input-decoupling zeros $z_{i1} = 2$, $z_{i2} = 3$ and has no input-output decoupling zeros.

The transfer function of the positive and standard system is equal to zero.

Consider the positive pair

$$A = \begin{bmatrix} 0 & 1 & 0 & ... & 0 \\ 0 & 0 & 1 & ... & 0 \\ \vdots & \vdots & \vdots & \ddots & \vdots \\ 0 & 0 & 0 & ... & 1 \\ a_0 & a_1 & a_2 & ... & a_{n-1} \end{bmatrix} \in \Re_+^{n \times n}, \quad B = \begin{bmatrix} 0 \\ 1 \\ 0 \\ \vdots \\ 0 \end{bmatrix} \in \Re_+^n \quad (4.19)$$

with $a_0 = a_1 = 0$.

The reachability matrix of the pair (4.19)

$$R_n = [B \quad AB \quad ... \quad A^{n-1}B] = \begin{bmatrix} 0 & 1 & 0 & ... & 0 \\ 1 & 0 & 0 & ... & 0 \\ 0 & 0 & 0 & ... & 0 \\ \vdots & \vdots & \vdots & ... & \vdots \\ 0 & 0 & 0 & ... & 0 \end{bmatrix} \in \Re_+^{n \times n} \quad (4.20)$$

has rank equal to two and two linearly independent monomial columns.

In this case the monomial matrix (3.4) has the form

$$P = [P_1 \quad ... \quad P_n] = \begin{bmatrix} 0 & 1 & 0 & ... & 0 \\ 1 & 0 & 0 & ... & 0 \\ 0 & 0 & 1 & ... & 0 \\ \vdots & \vdots & \vdots & \ddots & \vdots \\ 0 & 0 & 0 & ... & 1 \end{bmatrix} \in \Re_+^{n \times n} \quad (4.21)$$

and the assumption (3.5) is satisfied since

$AP_2 = [0 \quad ... \quad 0]^T$ and $P_k^T AP_2 = 0$ for $k = 3,\ldots,n$.

Using (3.6) and (4.21) we obtain

$$\bar{A} = P^{-1}AP = \begin{bmatrix} 0 & 1 & 0 & ... & 0 \\ 1 & 0 & 0 & ... & 0 \\ 0 & 0 & 1 & ... & 0 \\ \vdots & \vdots & \vdots & \ddots & \vdots \\ 0 & 0 & 0 & ... & 1 \end{bmatrix} \begin{bmatrix} 0 & 1 & 0 & ... & 0 \\ 0 & 0 & 1 & ... & 0 \\ \vdots & \vdots & \vdots & \ddots & \vdots \\ 0 & 0 & 0 & ... & 1 \\ a_0 & a_1 & a_2 & ... & a_{n-1} \end{bmatrix}$$

$$\begin{bmatrix} 0 & 1 & 0 & ... & 0 \\ 1 & 0 & 0 & ... & 0 \\ 0 & 0 & 1 & ... & 0 \\ \vdots & \vdots & \vdots & \ddots & \vdots \\ 0 & 0 & 0 & ... & 1 \end{bmatrix} = \begin{bmatrix} \bar{A}_1 & \bar{A}_{12} \\ 0 & \bar{A}_2 \end{bmatrix},$$

$$\bar{A}_1 = \begin{bmatrix} 0 & 0 \\ 1 & 0 \end{bmatrix} \in \Re_+^{2 \times 2}, \quad \bar{A}_{12} = \begin{bmatrix} 1 & 0 & ... & 0 \\ 0 & 0 & ... & 0 \end{bmatrix} \in \Re_+^{2 \times (n-2)},$$

$$\bar{A}_2 = \begin{bmatrix} 0 & 1 & 0 & ... & 0 \\ 0 & 0 & 1 & ... & 0 \\ \vdots & \vdots & \vdots & \ddots & \vdots \\ 0 & 0 & 0 & ... & 1 \\ a_2 & a_3 & a_4 & ... & a_{n-1} \end{bmatrix} \in \Re_+^{(n-2) \times (n-2)} \quad (4.22a)$$

and

$$\bar{B} = P^{-1}B = \begin{bmatrix} 0 & 1 & 0 & ... & 0 \\ 1 & 0 & 0 & ... & 0 \\ 0 & 0 & 1 & ... & 0 \\ \vdots & \vdots & \vdots & \ddots & \vdots \\ 0 & 0 & 0 & ... & 1 \end{bmatrix} \begin{bmatrix} 0 \\ 1 \\ 0 \\ \vdots \\ 0 \end{bmatrix} = \begin{bmatrix} \bar{B}_1 \\ 0 \end{bmatrix}, \ \bar{B}_1 = \begin{bmatrix} 1 \\ 0 \end{bmatrix} \in \Re_+^2 \quad (4.22b)$$

Theorem 4.1. If the rank of the reachability matrix (4.20) is equal to the number of linearly independent monomial columns then the input-decoupling zeros of the standard and positive system with (4.19) are the same and they are the eigenvalues of the matrix $\bar{A}_2$. The state vector x_i of the system is independent of the input-decoupling zeros for any input u_i and zero initial conditions ($x_0 = 0$).

Proof. By Definition 4.1 the input-decoupling zeros are the eigenvalues of the matrix $\bar{A}_2$ and they are the same for standard and positive system since the similarity transformation matrix P has in both cases the same form (4.21). If the initial conditions are zero then the zet transformation of x_i is given by

$$X(z) = P^{-1}\bar{X}(z) = P^{-1}[Iz - \bar{A}]^{-1}\bar{B}U(z)$$

$$= P^{-1}\begin{bmatrix} Iz - \bar{A}_1 & -\bar{A}_{12} \\ 0 & Iz - \bar{A}_2 \end{bmatrix}^{-1}\begin{bmatrix} \bar{B}_1 \\ 0 \end{bmatrix}U(s) \quad (4.23)$$

$$= P^{-1}\begin{bmatrix} [Iz - \bar{A}_1]^{-1}\bar{B}_1 \\ 0 \end{bmatrix}U(z) = \begin{bmatrix} 1 \\ z^{-1} \\ 0 \\ \vdots \\ 0 \end{bmatrix}U(z)$$

where $U(z)$ is the zet transform of u_i.

Dual result we obtain for the positive pair

$$A = \begin{bmatrix} 0 & 0 & ... & 0 & a_0 \\ 1 & 0 & ... & 0 & a_1 \\ 0 & 1 & ... & 0 & a_2 \\ \vdots & \vdots & \ddots & \vdots & \vdots \\ 0 & 0 & ... & 1 & a_{n-1} \end{bmatrix} \in \Re_+^{n \times n}, \quad (4.24)$$

$$C = [0 \quad 1 \quad 0 \quad ... \quad 0] \in \Re_+^{1 \times n}$$

with $a_0 = a_1 = 0$.

The observability matrix of the pair (4.24)

$$O_n = \begin{bmatrix} C \\ CA \\ \vdots \\ CA^{n-1} \end{bmatrix} = \begin{bmatrix} 0 & 1 & 0 & ... & 0 \\ 1 & 0 & 0 & ... & 0 \\ 0 & 0 & 0 & ... & 0 \\ \vdots & \vdots & \vdots & ... & \vdots \\ 0 & 0 & 0 & ... & 0 \end{bmatrix} \in \Re_+^{n \times n} \quad (4.25)$$

has rank equal to two and two linearly independent monomial rows.

In this case the monomial matrix (3.10) has the form

$$P = \begin{bmatrix} Q_1 \\ \vdots \\ Q_n \end{bmatrix} = \begin{bmatrix} 0 & 1 & 0 & ... & 0 \\ 1 & 0 & 0 & ... & 0 \\ 0 & 0 & 1 & ... & 0 \\ \vdots & \vdots & \vdots & \ddots & \vdots \\ 0 & 0 & 0 & ... & 1 \end{bmatrix} \in \Re_+^{n \times n} \quad (4.26)$$

and the assumption (3.11) is satisfied since
$Q_2 A = [0 \quad ... \quad 0]$ and $Q_2 A Q_k = 0$ for $k = 3,\ldots,n$.

Using (3.12) and (4.25) we obtain

$$\hat{A} = QAQ^{-1} = \begin{bmatrix} 0 & 1 & 0 & ... & 0 \\ 1 & 0 & 0 & ... & 0 \\ 0 & 0 & 1 & ... & 0 \\ \vdots & \vdots & \vdots & \ddots & \vdots \\ 0 & 0 & 0 & ... & 1 \end{bmatrix} \begin{bmatrix} 0 & 0 & ... & 0 & a_0 \\ 1 & 0 & ... & 0 & a_1 \\ 0 & 1 & ... & 0 & a_2 \\ \vdots & \vdots & \ddots & \vdots & \vdots \\ 0 & 0 & ... & 1 & a_{n-1} \end{bmatrix} \begin{bmatrix} 0 & 1 & 0 & ... & 0 \\ 1 & 0 & 0 & ... & 0 \\ 0 & 0 & 1 & ... & 0 \\ \vdots & \vdots & \vdots & \ddots & \vdots \\ 0 & 0 & 0 & ... & 1 \end{bmatrix} = \begin{bmatrix} \hat{A}_1 & 0 \\ \hat{A}_{21} & \hat{A}_2 \end{bmatrix},$$

$$\hat{A}_1 = \begin{bmatrix} 0 & 1 \\ 0 & 0 \end{bmatrix} \in \Re_+^{2 \times 2}, \quad \hat{A}_{21} = \begin{bmatrix} 1 & 0 \\ 0 & 0 \\ \vdots & \vdots \\ 0 & 0 \end{bmatrix} \in \Re_+^{(n-2) \times 2},$$

$$\hat{A}_2 = \begin{bmatrix} 0 & 0 & ... & 0 & a_2 \\ 1 & 0 & ... & 0 & a_3 \\ 0 & 1 & ... & 0 & a_4 \\ \vdots & \vdots & \ddots & \vdots & \vdots \\ 0 & 0 & ... & 1 & a_{n-1} \end{bmatrix} \in \Re_+^{(n-2) \times (n-2)} \quad (4.27a)$$

and

$$\hat{C} = CQ^{-1} = [0 \quad 1 \quad 0 \quad ... \quad 0] \begin{bmatrix} 0 & 1 & 0 & ... & 0 \\ 1 & 0 & 0 & ... & 0 \\ 0 & 0 & 1 & ... & 0 \\ \vdots & \vdots & \vdots & \ddots & \vdots \\ 0 & 0 & 0 & ... & 1 \end{bmatrix} = [1 \quad 0 \quad ... \quad 0] = [\hat{C}_1 \quad 0], \quad \hat{C}_1 = [1 \quad 0] \in \Re_+^{1 \times 2} \quad (4.27b)$$

Theorem 4.2. If the rank of the observability matrix (4.25) is equal to the number of linearly independent monomial rows then the output-decoupling zeros of the standard and positive system with (4.24) are the same and they are the eigenvalues of the matrix $\hat{A}_2$. The output y_i of the system is independent of the output-decoupling zeros for any input $u_i' = Bu_i$ and zero initial conditions ($x_0 = 0$).

Proof is similar (dual) to the proof of Theorem 4.1.

Example 4.5. For the positive pair

$$A = \begin{bmatrix} 0 & 0 & 0 \\ 1 & 0 & 0 \\ 0 & 1 & a \end{bmatrix}, \quad (a > 0), \quad C = [0 \quad 1 \quad 0] \quad (4.28)$$

the matrix (4.26) has the form

$$Q = \begin{bmatrix} 0 & 1 & 0 \\ 1 & 0 & 0 \\ 0 & 0 & 1 \end{bmatrix}. \quad (4.29)$$

Using (3.12) and (4.29) we obtain

$$\hat{A} = QAQ^{-1} = \begin{bmatrix} 0 & 1 & 0 \\ 0 & 0 & 0 \\ 1 & 0 & a \end{bmatrix} = \begin{bmatrix} \hat{A}_1 & 0 \\ \hat{A}_{21} & \hat{A}_2 \end{bmatrix}, \quad (4.30a)$$

$$\hat{A}_1 = \begin{bmatrix} 0 & 1 \\ 0 & 0 \end{bmatrix}, \quad \hat{A}_{21} = [1 \quad 0], \quad \hat{A}_2 = [a]$$

and

$$C = CQ^{-1} = [1 \quad 0 \quad 0] = [\hat{C}_1 \quad 0], \quad \hat{C}_1 = [1 \quad 0] \quad (4.30b)$$

The pair $(\hat{A}_1, \hat{C}_1)$ is observable since $\begin{bmatrix} \hat{C}_1 \\ \hat{C}_1 \hat{A}_1 \end{bmatrix} = \begin{bmatrix} 1 & 0 \\ 0 & 1 \end{bmatrix}$ and the positive system has one ouput-decoupling zero $z_{01} = a$.

The zet transform of the output for $x_o = 0$ and $U'(z) = BU(z)$ is given by

$$\begin{aligned} T(s) &= C[I_n z - A]^{-1} U'(z) \\ &= \hat{C}[I_n z - \hat{A}]^{-1} U'(z) = z^{-1} U'(z) \end{aligned} \quad (4.31)$$

and it is independent of the output-decoupling zero.

The presented results can be extended to multi-input multi-output discrete-time linear systems as follows.

Theorem 4.3. Let the reachability matrix (3.1) of the positive system (2.1) have rank equal to its $n_1 < n$ line-

arly independent monomial columns and the assumption (3.5) be satisfied. Then the input-decoupling zeros of the standard and positive system are the same and they are the eigenvalues of the matrix $\overline{A}_2$. The state vector x_i of the system is independent of the input-decoupling zeros for any input vector u_i and zero initial conditions.

Proof. If the reachability matrix (3.1) of the system (2.1) has rank equal to its n_1 linearly independent monomial columns and the assumption (3.5) is satisfied then the similarity transformation matrix P has the same form for standard and positive system. In this case the matrix $\overline{A}_2$ is the same for standard and positive system. Therefore, the input-decoupling zero for the standard and positive system is the same. The second part of the Theorem can be proved in a similar way as of Theorem 4.1.

Theorem 4.4. Let the observability matrix (3.9) of the positive system (2.1) has rank equal to its $n_1 < n$ linearly independent monomial rows and the assumption (3.11) be satisfied. Then the output-decoupling zeros of the standard and positive system are the same and they are the eigenvalues of the matrix $\hat{A}_2$. The output vector y_i of the system is independent of the output-decoupling zeros for any input vector $u_i' = Bu_i$ and zero initial conditions.

Remark 4.1. Note that if the positive pair (A,B) can be decomposed then the corresponding standard pair (A,B) can also be decomposed. Therefore, if the positive system (2.1) has input-decoupling zeros then the standard system (2.1) has also input-decoupling zeros.

Similar (dual) remark we have for the pair (A,C) and the output-decoupling zeros.

The following example shows that the positive system (2.1) may not have input-decoupling zeros but the standard system has input-decoupling zeros.

Example 4.6. The reachability matrix for the positive pair

$$A = \begin{bmatrix} 1 & 2 & 1 \\ 0 & 1 & 0 \\ 1 & 3 & 1 \end{bmatrix}, \quad B = \begin{bmatrix} 1 \\ 0 \\ 1 \end{bmatrix} \tag{4.32}$$

has the form

$$[B \quad AB \quad A^2B] = \begin{bmatrix} 1 & 2 & 4 \\ 0 & 0 & 0 \\ 1 & 2 & 4 \end{bmatrix}. \tag{4.33}$$

It has no monomial columns and it can not be decomposed (as the positive pair) but it can be decomposed as a standard pair since the rank of the reachability matrix (4.33) is equal to one. The similarity transformation matrix has the form

$$P = \begin{bmatrix} 1 & 0 & 0 \\ 0 & 1 & 0 \\ 1 & 0 & 1 \end{bmatrix} \tag{4.34}$$

and we obtain

$$\overline{A} = P^{-1}AP = \begin{bmatrix} 2 & 2 & 1 \\ 0 & 1 & 0 \\ 0 & 1 & 0 \end{bmatrix} = \begin{bmatrix} \overline{A}_1 & \overline{A}_{12} \\ 0 & \overline{A}_2 \end{bmatrix}, \tag{4.35a}$$

$$\overline{A}_1 = [2], \quad \overline{A}_{12} = [2 \quad 1], \quad \overline{A}_2 = \begin{bmatrix} 1 & 0 \\ 1 & 0 \end{bmatrix}$$

$$\overline{B} = P^{-1}B = \begin{bmatrix} 1 \\ 0 \\ 0 \end{bmatrix} = \begin{bmatrix} \overline{B}_1 \\ 0 \end{bmatrix}, \quad \overline{B}_1 = [1] \tag{4.35b}$$

The matrix $\overline{A}_2$ has the eigenvalues $z_{i1} = 1$, $z_{i2} = 0$. Therefore, the positive system with (4.32) has not input-decoupling zeros but it has input-decoupling zeros ($z_{i1} = 1$, $z_{i2} = 0$) as a standard system.

5. Concluding Remarks

The notions of the input-decoupling zero, output-decoupling zero and input-output decoupling zero for positive discrete-time linear systems have been introduced. The necessary and sufficient conditions for the reachability (observability) of positive linear systems are much stronger than the conditions for standard linear systems (Theorem 2.2 and 2.4). The conditions for decomposition of positive system are also much stronger than for the standard systems. Therefore, the conditions for the existence of decoupling zeros of positive systems are more restrictive. It has been shown that: 1) if the positive system has decoupling zeros then the corresponding standard system has also decoupling zeros, 2) the positive system may not have decoupling zeros when the corresponding standard system has decoupling zeros (Example 4.6), 3) the positive and standard system have the same decoupling zeros if the rank of reachability (observability) matrix is equal to the number of linearly independent monomial columns (rows) and the assumption (3.5) ((3.11)) is satisfied (Theorem 4.3 and 4.4).

The considerations have been illustrated by numerical examples. Open problems are extension of these considerations to positive continuous-time linear systems and to positive 2D linear systems.

6. References

[1] L. Farina and S. Rinaldi, "Positive Linear Systems, Theory and Applications," Wiley, New York, 2000.

[2] T. Kaczorek, "Positive 1D and 2D Systems," Springer Verlag, London, 2001.

[3] R. E. Kalman, "Mathematical Descriptions of Linear Systems," *SIAM Journal on Control*, Vol. 1, No. 2, 1963, pp. 152-192.

[4] R. E. Kalman, "On the General Theory of Control Sys-

tems," *Proceedings of the First International Congress on Automatic Control*, Butterworth, London, 1960, pp. 481-493.

[5] P. J. Antsaklis and A. N. Michel, "Linear Systems," Birkhauser, Boston, 2006.

[6] T. Kaczorek, "Linear Control Systems," Vol. 1, Wiley, New York, 1993.

[7] T. Kailath, "Linear Systems," Prentice-Hall, Englewood Cliffs, New York, 1980.

[8] H. H. Rosenbrock, "State-Space and Multivariable Theory," Wiley, New York, 1970.

[9] W. A. Wolovich, "Linear Multivariable Systems," Springer-Verlag, New York, 1974.

[10] T. Kaczorek, "Reachability and Controllability to Zero Tests for Standard and Positive Fractional Discrete-Time Systems," *Journal Européen des Systèmes Automatisés*, Vol. 42, No. 6-8, 2008, pp. 770-781.

[11] T. Kaczorek, "Decomposition of the Pairs (A,B) and (A,C) of the Positive Discrete-Time Linear Systems," *Proceedings of TRANSCOMP*, Zakopane, 6-9 December 2010.

[12] H. H. Rosenbrock, "Comments on Poles and Zeros of Linear Multivariable Systems: A Survey of the Algebraic Geometric and Complex Variable Theory," *International Journal on Control*, Vol. 26, No. 1, 1977, pp. 157-161.

Circuits and Systems, **2010, 1, 49-53**
doi:10.4236/cs.2010.12008 Published Online October 2010 (http://www.SciRP.org/journal/cs)

Designing Parameters for RF CMOS Cells

Viranjay M. Srivastava[1], K. S. Yadav[2], G. Singh[1]
[1]*Department of Electronics and Communication Engineering, Jaypee University of Information Technology, Solan, India*
[2]*VLSI Design Group, Central Electronics Engineering Research Institute* (*CEERI*), *Pilani, India*
E-mail: *viranjay@ieee.org*
Received July 29, 2010; *revised August* 30, 2010; *accepted September* 5, 2010

Abstract

In this paper, we have investigated the design parameters of RF CMOS cells which will be used for switch in the wireless telecommunication systems. This RF switch is capable to select the data streams from the two antennas for both the transmitting and receiving processes. The results for the development of a cell-library which includes the basics of the circuit elements required for the radio frequency sub-systems of the integrated circuits such as V-I characteristics at low-voltages, contact resistance which is present in the switches and the potential barrier with contacts available in devices has been discussed.

Keywords: CMOS, Cell Library, Contact Resistance, DG MOSFET, DP4T Switch, Potential Barrier, Radio Frequency, RF Switch, Resistance of MOS, Voltage-Current Curve, VLSI

1. Introduction

Earlier, the radio transceiver switches have been designed using PIN diodes, which consumes more power. As the modern portable devices demands less-power consumption switches, therefore, the PIN diodes are gradually replaced by the Metal Oxide Semiconductor Field Effect Transistors (MOSFET) such as the n-type MOS and p-type MOS [1,2]. A traditional NMOS switch has better performances but only for a single operating frequency. For multiple operating frequencies, high signal distortions are easily observed, which results in an unrecognizable information signal at the receiver end which would be measured by using the curve of capacitance and voltage with VEE Pro software [3,4]. The aggressive scaling of metal-oxide-semiconductor field effect transistors (MOSFET) has led to the fabrication of high performance MOSFETs with a cutoff frequency f_T of more than 150 GHz [5]. As a result of this development, the CMOS is a strong candidate for RF wireless communications in the GHz frequency range. Accurate device models are, however, needed to design the advanced analogue RF circuits and for this regards, various researcher propose some parameters for cell design as used for RF switch circuits [6,7].

Continuous scaling of CMOS technology has now reached a state of evolution, in terms of both frequency and noise, where it is becoming a severe part for RF applications in the GHz frequency range. To be able to transmitting or receiving information through the multiple antennas systems, known as MIMO systems, it becomes necessary to design a new RF switch that is capable of operating with multiple antennas and frequencies as well as minimizing signal distortions and power consumption [8-10].

The use of analog CMOS circuits at high frequency have more attention in the last several years, with many applications focused on the growing commercial market as RF switch, DP4T RF CMOS switch [11,12]. Modern consumer products require cost competitive technology and RF CMOS has proven to be cost-effective and high volume technology. CMOS is also best suitable to integrate RF with digital circuits making it possible to build a system on a single chip. Due to these advantages, there has been growing interest in modeling of RF CMOS which is especially striking for many applications because it allows integration of both digital and analog functionality on the same die, increasing performance at the same time as keeping system sizes reserved. Applications for a CMOS switch also covers the areas of micro power circuits and other wireless applications at frequencies from as low as 100 MHz for low earth orbiting satellite system to thousand of MHz [13-16]. Various circuit parameters have been discussed in this paper for better performance.

Rapid integrated system designs are the use of cell li-

braries for various system functions [15,17]. In digital system design, these standard cells are both at the logic primitive level (for example NAND and NOR gates) as well as higher levels of circuit functionality (for example, ALU, memory). For baseband analog systems, standard cell libraries are less frequently used. In the design of a CMOS RF cell library, the cells must be designed to be flexible in terms of drive requirements, bandwidth and circuit loading. For RF applications, the most common drive requirements for off-chip loads are based on 50 Ω impedances. This impedance is a good compromise between lowest loss and highest power handling for a given cable size. Also this impedance caught on for RF transmission rather than the well established 75 Ω that had been used for video transmission. A factor governing the bandwidth of the RF cells is the nodal capacitance to ground, primarily the drain and source sidewall capacitances [18,19]. Since these cells are to be used with digital and baseband analog systems, control by on-chip digital and analog signals is another factor in the design [20].

The library consists of cells designed, using standard Micro-Cap 2.0 μm and 0.8 μm CMOS processes. For the technologies studied, these control voltages varied between 0.3 V and 5.0 V, with the supply voltage of 1.2 V is of interest for low power consumption portable system applications. The cells have been designed for the purpose of radio frequency communication switch devices. In the design of cell library for digital and analog, a swapping between speed and frequency response and circuit complexity is always encountered. Transistors making for the purpose of library elements are usually planned with multiple gate fingers to reduce the capacitances of sidewall. This increases the contact resistance and reduces the barrier height. The properties for RF CMOS switch design for the application in communication and designed results are presented and have been designed with and optimized for the particular application [12].

Each of the cells parameters will be discussed separately for the purpose of clarity of presentation and understanding of the operation of the circuit. The organization of the paper is as follows. Voltage-current curve at low voltages for application in RF switches are discussed in Section 2, contact resistances present in switch are discussed in Section 3, the potential barrier with contacts are discussed in Section 4 and at last conclusion is in Section 5.

2. V – I Characteristics of RF CMOS

The selection of RF CMOS transistors requires an analysis of performance specifications. Since drain-source breakdown voltage is the maximum drain to source voltage before breakdown with the gate grounded [21], also specifications for RF CMOS transistors include maximum drain saturation, common-source forward transconductance, operating frequency, and output power. RF MOSFET transistors vary in terms of operating mode, packaging, and packing methods. Devices that operate in depletion mode can increase or decrease their channels by an appropriate gate voltage. By contrast, devices that operate in enhancement mode can only increase their channels by an appropriate gate voltage. In terms of packaging, RF MOSFET transistors are available in small outline (SO), transistor outline (TO), small outline transistor (SOT), and flat packaging (FPAK). Devices use either surface mount technology (SMT) or through hole technology (SMT) and vary in terms of the number of leads.

This paper proposes a design of RF CMOS cells for low power consumption and low distortion for application of RF switch in communication that operates at 2.4 GHz and 5.0 GHz [20]. n-channel devices were used in the HF portion of the circuits with p-channel devices used as current sources. The cells which were designed here are to drive 50 Ω resistive loads and utilized multiple gate fingers to reduce parasitic capacitance in an effort to improve the operating frequency.

The gate metal contact forms a MOS contact with the substrate which exist below the oxide insulator. When a voltage is applied to the gate terminal, and as it rises above the threshold of the MOS contact then an inversion layer, a channel is created in the substrate and the properties of semiconductor will be interchanged between p-type to n-type properties. The ideal threshold voltage is determined by,

$$V_T = \frac{\sqrt{2\varepsilon_S q N_A (2\psi_B)}}{C_0} + 2\psi_B \tag{1}$$

where ψ_B, N_A, and C_o are the surface potential to cause an inversion layer, the semiconductor doping concentration in channel/substrate and capacitance of the oxide layer respectively [22]. The surface potential to cause an inversion layer, ψ_S (inv), is given by the equation,

$$\psi_S(inv) \approx 2\psi_B = \frac{2kT}{q} \ln\left(\frac{N_A}{n_i}\right) \tag{2}$$

where k, T, q, N_A, and n_i are Boltzmann constant, absolute temperature, electronic charge, number of doping molecules and intrinsic concentration respectively. After the inversion layer formed, a drain voltage is applied to MOSFET. As in the linear region, drain voltage is undersized also at this inversion layer has a constant resistance because of the linear V-I characteristics. A depletion region forms between the inversion layer in the channel of the MOSFET, and the drain well as the volt-

age difference from the drain to gate increases to more than V_T. This causes the current to reach a maximum current (saturation current, $I_{Dsat,}$).

For the fabricated device with gate oxide thickness (t_{ox}) 650 Å, oxide capacitance (C_{ox}) $5.31*10^{-8}$ F/cm^2 [23], channel length (L) 0.8 µm, channel width (W) 400 µm, mobility 800 cm^2/V-s, channel doping (N_B) 10^{15}/cm^3 so we found the V_{th} 0.867 V and found the drain current as shown in **Figure 1** with different drain voltage range. Similarly, with the gate voltage range (V_G) 0.3 V to 2.1 V, step size 0.3 V drain voltage range (V_D) 0 V to 1.5 V, we found the drain current 3.8 mA for V_G 1.5 V, 8.0 mA for V_G 1.8 V, and 13.6 mA for V_G 2.1 V.

A RF CMOS has the properties as fixed tuned matching networks, low Q matching networks, ruggedness, high power output, mounting flange packages, and Silicon grease. Power gain (a measure of power amplification, is the ratio of output power to input power, dB), Noise figure (a measure of the amount of noise added during normal operation, is the ratio of the signal-to-noise ratio at the input and the signal-to-noise ratio at the output, dB), High power dissipation (a measure of total power consumption, W or mW). Some bipolar RF CMOS transistors are suitable for automotive, commercial or general industrial applications.

3. Contact Resistances

For measuring the contact resistance of a metal-semiconductor junction of MOSFET, deposition of metal on the semiconductor are required and it patterns, so that various identical pads spaced with different distances as shown in **Figure 2**.

These patterns include many rows of different pad sizes. The pads in any one row should be of same size, whereas the distances between pads are varying. The measurements required simple voltage and current curves.

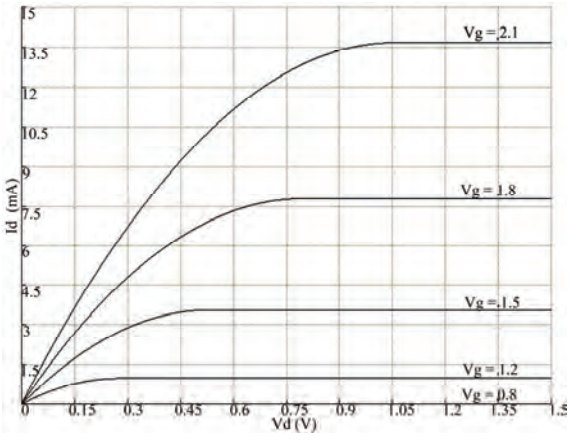

Figure 1. Gate voltage range (V_G) = 0.3 V to 1.2 V, step size = 0.1 V, drain voltage range (V_D) = 0 to 0.5 V.

For calculating the resistance, we apply a voltage between some pairs of adjoining pads in of a row, and measure the current flow. From this, calculate the resistance between those two pads. As shown in **Figure 2**, the total resistance between any two pads is the series combination of following three resistors; metal to semiconductor, through the semiconductor and back into metal. Since ohmic contacts are the same for both polarities, so $R = 2R_{pad} + R_{semi}$ as shown in **Figure 3**.

When the distance between two pads tends to zero, then resistance through the semiconductor (R_{semi}) goes to zero and only resistance between metal to semiconductor and back into metal will be left ($2R_{pad}$). Now we have R_{pad}, multiply that value by the area of the metal pads (in cm^2). For author's circuit it is taken as 10^{-5} Ω-cm^2. Consider that in the modern processes, the vias that contact the silicon have a contact area of about 0.1 µm^2 or 10^{-8} cm^2. If contact resistance is 10^{-5} Ωcm^2, that amounts to 1.0 kΩ resistor to get into the silicon (plus another to get out). A good contact resistance is on the order of 10^{-7} Ωcm^2.

The Schottky contact resistance between the silicide layer and polysilicon is the most likely cause of the excessive gate resistance and as measured using above techniques. The contact resistance values, which are in good agreement with the result as shown in **Figure 3**, for monolithic silicon, were shown to contribute substantially to the gate resistance. Downscaling of CMOS technologies will make the problem more pronounced, since the interface contact resistance is inversely proportional to the total gate area as in term of length and width of a gate. The reduction of resistance should lead to improved RF

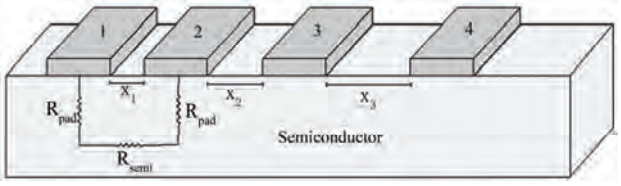

Figure 2. Example of the metal pattern of a RF MOSFET.

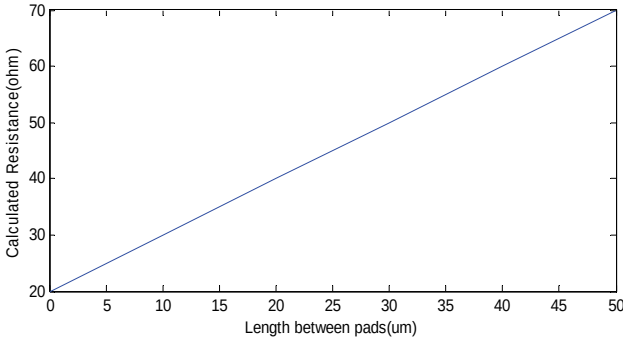

Figure 3. Resistance variation with pad lengths.

properties in MOSFETs [6,24,25].

4. Potential Barriers

Potential barrier exist between metal and semiconductor layer when they are in close contact, this stops the majority of charge carriers to pass from one layer to the other layer. Only a few charge carriers have an adequate amount of energy to pass though the barrier and cross to the other side material. After applying a bias voltage to the junction, it has following two effects, first it can create the barrier come into view lower from the semiconductor side, or second, it can make so higher. But the bias does not change the barrier height from the metal side. This creates a Schottky Barrier also known as rectifying contact, where junction conducts only for one bias polarity, not the other. This rectifying contact makes good diodes and can even be used to make a kind of transistor.

A direct method of potential barrier height determination is presented in this section. The best agreement between the barrier heights determined this method using a dependence of the Si-SiO_2 interface barrier height on the thickness of the aluminium gate has been observed [15]. Since the barrier height is the property of a material, so we try to use these materials for the CMOS in application of RF, whose barrier height is small. Here is a possibility to create an alloy between metal and semiconductor junction, at the time of annealing, which lowers the barrier height [26]. The probability of tunneling becomes high for extremely thin barriers (in the tens of nanometers). By the heavy doping process one can make the very thin barrier which is approximately doing concentration of 10^{19} dopant atoms/cm^3 or more.

As the barrier height is closer to zero, ohmic contact increases. For this one can concludes the following result as shown in **Table 1**, for a positive barrier height.

Aluminium (*Al*), for doping of polysilicon 10^{15}/cm^3, n-type, p-Silicon, semiconductor barrier height will 0.92 eV and metal-semiconductor junction depletion layer width is 0.284 μm wide.

Ploysilicon, doping of polysilicon 10^{15}/cm^3, n-type, p-Silicon, semiconductor barrier height will 0.85 eV and metal-semiconductor junction depletion layer width is 0 wide.

So for the polysilicon, we achieve the barrier height is closer to zero, which increases the ohmic contact.

Table 1. Direction of current flow.

Type	Current flow into (easily)
n	semiconductor
p	metal

5. Results and Conclusions

After calculation of the currents, resistance and potential barrier, we conclude that the drain current increases with increase of the gate voltage or control voltage. Also, the MOS device parameters can be used with VEE Programming [27]. For the purpose of RF switch, where control voltage should be low and then current flow will be less and in terms of contact resistance, it will increases with increase in number of gate fingers. So in application of RF switch authors have tried to lower the gate finger. The semiconductor barrier height and depletion layer width is more for aluminum compare to polysilicon metal-semiconductor junction which is 0.284 μm wide. Since the operating frequencies of the RF switches are in the order of GHz, therefore, it is useful for wireless local area network (WLAN) and other IEEE 802.11 applications.

6. Acknowledgements

The authors would like to thank Prof. A. B. Bhattacharaya, Jaypee Institute of Information Technology, India and Mr. Peeyush Tripathi, Intel Corporation, Bangalore, India for insightful discussions.

7. References

[1] Skyworks Solutions Inc., "Application Note, APN1002, Design with PIN Diodes," Woburn, July 2005.

[2] J. Park and Z. Q. Ma, "A 15 GHz CMOS RF Switch Employing Large Signal Impedance Matching," *Proceeding of Topical Meeting on Silicon Monolithic Integrated Circuits in RF Systems*, Denver, 2006, pp. 1-4.

[3] M. Viranjay Srivastava, K. S. Yadav and G. Singh, "Application of VEE Pro Software for Measurement of MOS Device Parameter Using C-V Curve," *International Journal of Computer Applications*, Vol. 1, No. 7, March 2010, pp. 43-46.

[4] V. M. Srivastava, "Capacitance-Voltage Measurement for Characterization of a Metal Gate MOS Process," *International Journal of Recent Trends in Engineering*, Vol. 1, No. 4, May 2009, pp. 4-7.

[5] A. Litwin, E. Microelectron and A. B. Stockholm, "Overlooked Interfacial Silicide-Polysilicon Gate Resistance in MOS Transistors," *IEEE Transactions on Electron Devices*, Vol. 48, No. 9, September 2001, pp. 2179-2181.

[6] V. M. Srivastava, K. S. Yadav and G. Singh, "Attenuation with Double Pole Four Throw CMOS Switch Design," *IEEE International Conference on Semiconductor Electronics* (*ICSE*-2010), Malacca, 28-30 June 2010, pp. 173-175.

[7] Y. J. Chan, C. H. Huang, C. C. Weng and B. K. Liew,

"Characteristics of Deep Sub-Micrometer MOSFET and its Empirical Non-Linear RF Model," *IEEE Transaction on Microwave Theory*, Vol. 46, No. 5, May 1998, pp. 611-615.

[8] J. P. Carmo, P. M. Mendes, C. Couto and J. H. Correia "A 2.4-GHz RF CMOS Transceiver for Wireless Sensor Applications," *Proceeding of International Conference on Electrical Engineering*, Coimbra, 2005, pp. 902-905.

[9] P. Mekanand and D. Eungdamorang, "DP4T CMOS Switch in a Transceiver of MIMO System," *Proceeding of* 11*th IEEE International Conference of Advanced Communication Technology*, Korea, 2009, pp. 472-474.

[10] P. H. Woerlee, M. J. Knitel, R. V. Langevelde, D. B. Klaassen, L. F. Tiemeijer and A. J. Scholten, "RF CMOS Performance Trends," *IEEE Transaction on Electron Devices*, Vol. 48, No. 8, August 2001, pp. 1776-1782.

[11] T. H. Lee, "CMOS RF No Longer an Oxymoron," *Proceedings of the* 19*th Gallium Arsenide Integrated Circuit Symposium*, Anaheim, 1997, pp. 244-247.

[12] V. M. Srivastava, K. S. Yadav and G. Singh, "Double Pole Four Throw Switch Design with CMOS Inverter," *Proceeding of* 5*th IEEE International Conference on Wireless Communication and Sensor Network*, Kolkata, 15-19 December 2009, pp. 1-4.

[13] S. Lee, C. Yoo, W. Kim, H. K. Ryu and W. Song, "1 GHz CMOS Down Conversion Mixer," *Proceeding of IEEE International Symposium on Consumer Electronics*, Singapore, 1997, pp. 125-127.

[14] T. H. Lin, H. Sanchez, R. Rofougaran and W. J. Kaiser, "CMOS Front End Components for Micropower RF Wireless Systems," *Proceeding of International Symposium on Low Power Electronics and Design, Monterey*, California, 1998, pp. 11-15.

[15] F. Piazza, P. Orsatti, Q. Huang and T. Morimoto, "0.25 mm CMOS Transceiver Front-End for GSM," *Proceeding of IEEE Custom Integrated Circuits Conference*, Singapore, 1998, pp. 413-416.

[16] T. Manku, "Microwave CMOS Device Physics and Design," *IEEE Journal of Solid State Circuits*, Vol. 34, No. 3, March 1999, pp. 277-285.

[17] C. Laber, C. Rahim, S. Dreyer, G. Uehara, P. Kwok and P. Gray, "Design Considerations for a High Performance 3 Micron CMOS Analog Standard Cell Library," *IEEE Journal of Solid State Circuits*, Vol. 22, No. 2, 1987, pp. 181-189.

[18] Y. Cheng, and M. Matloubian, "Frequency Dependent Resistive and Capacitive Components in RF MOSFETs," *IEEE Electron Device Letters*, Vol. 22, No. 7, July 2001, pp. 333-335.

[19] K. J. Yang and C. Hu, "MOS Capacitance Measurements for High Leakage Thin Dielectrics," *IEEE Transaction on Electron Devices*, Vol. 46, No. 7, July 1997, pp. 1500-1501.

[20] M. Smith, C. Portman, C. Anagnostopoulos, P. Tschang, R. Rao, P. Valdenaire and H. Ching, "Cell Libraries and Assembly Tools for Analog/Digital CMOS and BiCMOS ASIC Design," *IEEE Journal of Solid State Circuits*, Vol. 24, No. 5, 1989, pp. 1419-1432.

[21] S. H. Lee, C. S. Kim and H. K. Yu, "A Small Signal RF Model and its Parameter Extraction for Substrate Effects in RF MOSFETs," *IEEE Transaction on Electron Devices*, Vol. 48, No. 7, July 2001, pp. 1374-1379.

[22] N. Talwalkar, C. Patrick Yue and S. Simon Wong, "Integrated CMOS Transmit-Receive Switch Using LC-Tuned Substrate Bias for 2.4 GHz and 5.2 GHz Applications," *IEEE Journal of Solid State Circuits*, Vol. 39, No. 6, 1989, pp. 863-870.

[23] V. M. Srivastava, K. S. Yadav and G. Singh, "Measurement of Oxide Thickness for MOS Devices, Using Simulation of SUPREM Simulator," *International Journal of Computer Applications*, Vol. 1, No. 6, March 2010, pp. 66-70.

[24] Y. Cheng and M. Matloubian, "Parameter Extraction of Accurate and Scaleable Substrate Resistace Components in RF MOSFETs," *IEEE Electron Device Letters*, Vol. 23, No. 4, April 2002, pp. 221-223.

[25] Y. S. Lin, S. S. Lu, T. S. Lee and H. B. Liang, "Characterization and Modeling of Small Signal Substrate Resistance Effect in RF CMOS," *IEEE MTT-S Digest*, June 2002, pp. 161-164.

[26] S. M. Sze, "Semiconductor Devices: Physics and Technology," 2nd Edition, Tata McGraw Hill, Noida, 2004.

[27] V. M. Srivastava, "Relevance of VEE Programming for Measurement of MOS Device Parameters," *Proceedings of IEEE International Advance Computing Conference*, Patiala, March 2009, pp. 205-209.

Circuits and Systems, **2010, 1, 54-58**
doi:10.4236/cs.2010.12009 Published Online October 2010 (http://www.SciRP.org/journal/cs)

SIMO Transadmittance Mode Active-C Universal Filter

Neeta Pandey[1], Sajal K. Paul[2*]
[1]*Department of Electronics and Communications, Delhi Technological University, Delhi, India*
[2]*Department of Electronics and Instrumentation, Indian School of Mines, Dhanbad, India*
E-mail: {*n66pandey, sajalkpaul*}*@rediffmail.com*
Received August 6, 2010; *revised September* 10, 2010; *accepted September* 13, 2010

Abstract

This paper presents two transadmittance mode universal filters having single voltage input and multiple current outputs. The filter employs three multiple output current controlled conveyors (MOCCCII) and two grounded capacitors. It can realize low pass, high pass, band pass, notch and all pass responses. As desired, the input voltage signal is inserted at high impedance input terminal and the output currents are obtained at high impedance output terminals and hence eases cascadability. The filter enjoys low sensitivity performance and low component spread; and exhibits electronic and orthogonal tunability of filter parameters via bias currents of MOCCCII. SPICE simulation results confirm the workability of the proposed structure.

Keywords: Universal Filter, Transadmittance Mode, Current Controlled Conveyor

1. Introduction

There has been substantial emphasis on development of current conveyor based filters in the recent past which can be attributed to its high performance properties such as wider signal bandwidths, greater linearity, larger dynamic range, lower power consumption, simple circuitry and occupy lesser chip area than their voltage mode counterparts [1]. The filters employing operational transconductance amplifier (OTA) possess lower dynamic range with power supply scaling as its input are voltage dependent. The need for lower power consumption requires low bias current and hence lower output current [2]. The OTA requires bias current of four times the current needed by current controlled conveyor (CCCII) [3] for the same transconductance. Thus circuits based on CCCII consume lesser power than OTA based circuits. The maximum usable frequency range depends strongly on bias current, hence high frequency response of CCCII based implementations are expected to be better than OTA. Already a number of voltage and current mode filter structures based on current conveyor have been reported in the literature [3-13] and references cited therein. A voltage-mode (VM) circuit is one whose signal states are computed as node voltages while a current-mode (CM) circuit is one whose signal states defined by its branch currents. In some applications there is need of filtering a voltage signal and then converting it to current signal by using a voltage to current converter (V→I) interfacing circuit. The total effectiveness of the electronic circuitry can be increased if signal processing can be combined with V→I interfacing. A transadmittance mode filter is suitable for such applications and finds usage in receiver base band blocks of modern radio system [14]. A careful study indicates that a limited literature is available on transadmittance mode filter [14-18]. These circuits can nicely perform the operation of transadmittance mode filter, but still there is scope to improve them in the following fronts: use of floating passive components [14-18] which is not considered good for IC implementation point of view; input voltages are not applied at high impedance terminal [14,16,18]; availability of output currents through passive components [17] thus there is requirement of additional hardware; and filter parameters are not electronically tunable [17]. It thus reveals that no literature is available on transadmittance mode universal filter that can simultaneously possess the following advantageous features: 1) use of all grounded passive components, 2) high impedance terminal for input excitation, 3) output at high impedance and 4) electronic tunability of filter parameters.

In this work, two current controlled conveyor based transadmittance mode universal filter circuits are proposed based on [10-13] that use only three MOCCCIIs and two grounded capacitors. The first structure provides band pass, high pass and notch responses simultaneously and all pass and low pass responses can be obtained by connecting together appropriate outputs. The low pass,

band pass, high pass and notch responses are simultaneously available in the second proposed structure and all pass response can be obtained by connecting together suitable outputs. As desired, in both the structures, the input voltage signal is inserted at high impedance input terminal and the output currents are obtained at high impedance output terminals. The filter parameters are adjustable through bias currents of MOCCCII. The filter, under all operations, exhibits low active and passive sensitivities. The function of the proposed structure has been confirmed by SPICE simulations.

2. Circuit Description

The port relationships of a MOCCCII as shown in **Figure 1** can be characterized by

$$v_X = v_Y + i_X \,|\, R_X(I_0)\,|, \quad i_Y = 0, \quad i_{Z\pm} = \pm i_X$$

where the positive and negative signs denote the positive and negative current transfers. R_x is the input resistance at x port which can be controlled via bias current I_0 [3]. The MOCCCII can be realized using bipolar transistor or CMOS (**Figure 2**), the value of R_x is given as $R_X = V_T / 2I_0$ for bipolar realization or MOS transistors operating in weak inversion region, where V_T is the thermal voltage; whereas $R_X = 1/(g_{m2} + g_{m4})$ for MOS transistors operating in strong inversion [19], where $g_{mi} = \sqrt{2\mu_i C_{ox}(W_i / L_i) I_0}$.

The first proposed transadmittance mode universal filter is shown in **Figure 3**, which employs three MOCCCIIs and two grounded capacitors. The routine analysis of the circuit yields the following transfer functions:

$$\frac{I_{out1}}{V_{in}} = -\frac{1}{R_{x1}D(s)}, \frac{I_{out2}}{V_{in}} = \frac{sC_2R_{x2}}{R_{x1}D(s)},$$

$$\frac{I_{out3}}{V_{in}} = -\frac{s^2C_1C_2R_{x2}}{D(s)}, \frac{I_{out4}}{V_{in}} = \frac{s^2C_1C_2R_{x1}R_{x2}+1}{R_{x1}D(s)} \qquad (1)$$

where $$D(s) = s^2C_1C_2R_{x1}R_{x2} + sC_2R_{x2} + 1 \qquad (2)$$

Thus the proposed structure of **Figure 3** can be viewed as single-input four-output transadmittance mode universal filter. It provides low pass, band pass, high pass and notch responses at I_{out1}, I_{out2}, I_{out3} and I_{out4} respectively. The all pass responses can easily be obtained by adding I_{out1}, I_{out2} and I_{out3}. Furthermore, the input voltage is applied at high impedance y-port and all the current outputs are available at high impedance z-port of current controlled conveyors that enable easy cascadability without the need of supplementary buffer circuit.

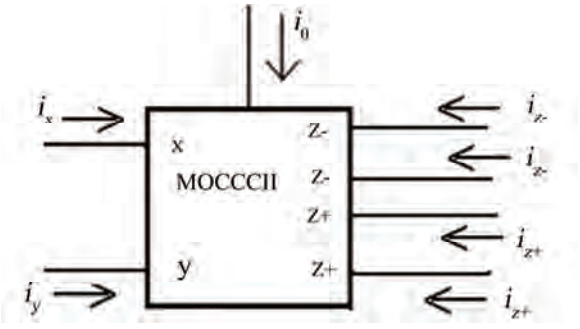

Figure 1. Circuit symbol of MOCCCII.

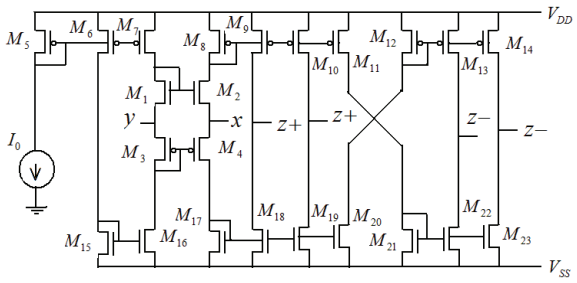

Figure 2. CMOS representation of MOCCCII [19].

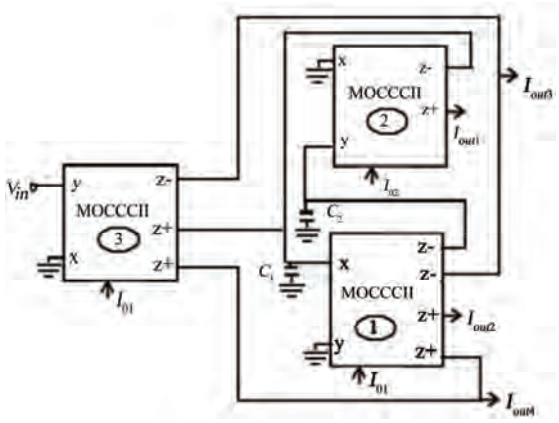

Figure 3. First proposed structure.

All the filters are characterized by

$$\omega_0 = \left(\frac{1}{R_{x1}R_{x2}C_1C_2}\right)^{1/2}, \quad \frac{\omega_0}{Q_0} = \frac{1}{R_{x1}C_1} \quad \text{and}$$

$$Q_0 = \left(\frac{R_{x1}C_1}{R_{x2}C_2}\right)^{1/2} \qquad (3)$$

It may be noted from (3) that ω_0 can be adjusted by varying bias current I_{02} (or R_{x2}) without disturbing ω_0 / Q_0 and similarly ω_0 and Q_0 are orthogonally adjustable with simultaneous adjustment of I_{01} and I_{02}.

The second proposed structure is shown in **Figure 4**, which uses two MOCCCIIs and a minus type CCCII and two grounded capacitors. The transfer functions for the circuit of **Figure 4** can be expressed as

$$\frac{I_{out1}}{V_{in}} = \frac{s^2C_1C_2R_{x2}}{D(s)}, \quad \frac{I_{out2}}{V_{in}} = \frac{sC_1}{D(s)}, \quad \frac{I_{out3}}{V_{in}} = \frac{D(s) - sC_1R_{x1}}{R_{x1}D(s)} \qquad (4)$$

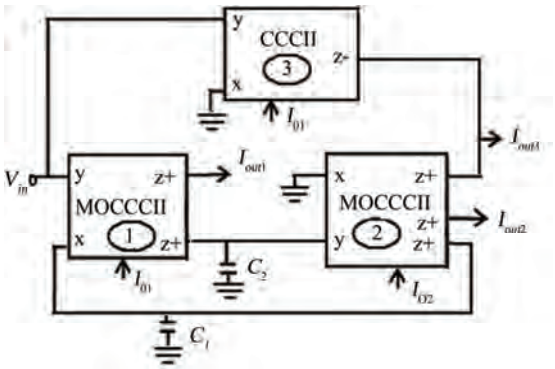

Figure 4. Second proposed structure.

where

$$D(s) = s^2 C_1 C_2 R_{x1} R_{x2} + sC_2 R_{x2} + 1 \qquad (5)$$

Thus the second structure can also be viewed as single-input three-output transadmittance mode universal filter. It provides high pass and band pass responses at I_{out1} and I_{out2}. The notch response is available at I_{out3} for equal capacitors $C_1 = C_2$ and bias currents $I_{01} = I_{02}$. The low pass and all pass responses can easily be obtained by adding I_{out1} and I_{out3}; and I_{out2} and I_{out3} respectively. Like the previous one, both the input and output impedances are high for input voltage and output currents respectively.

The results of active and passive sensitivity analysis of various parameters for both the proposed filters are given as

$$S_{R_{x1}}^{\omega_0} = S_{R_{x2}}^{\omega_0} = S_{C_1}^{\omega_0} = S_{C_2}^{\omega_0} = -1/2,$$

$$S_{R_{x1}}^{Q_0} = -S_{R_{x2}}^{Q_0} = S_{C_1}^{Q_0} = -S_{C_2}^{Q_0} = 1/2$$

Hence the sensitivities of pole ω_0 and quality factor Q_0 are low and within unity in magnitude. Thus the proposed structure can be classified as insensitive.

The Equation (3) also indicates that high values of Q-factor will be obtained from moderate values of ratios of passive components *i.e.*, from low component spread [20]. These ratios can be chosen as $(R_{x1}/R_{x2}) = (C_1/C_2) = Q_0$. Hence the spread of the component values becomes of the order of $\sqrt{Q_0}$. This feature of the filter related to the component spread allows the realization of high Q_0 values more accurately compares to the topologies where the spread of passive components becomes Q_0 or Q_0^2.

3. Comparison

Table 1 shows the comparison of the present work with the previously reported works [14-18]. The study of **Table 1** reveals the following.

1) [14] uses the same number of active components as that of present work, whereas the number of passive components are more in [14] and most of them are floating. Input impedance is low which is not desirable for a circuit having input as voltage signal. The NF and AP responses are not obtainable from this circuit.

2) [15] uses more number of active and passive components than that of the present work and most of the passive components are floating. Input impedance is low and NF and AP responses are not possible as that of [14].

3) Although [16] and [17] use single active component, the number of passive components are more and some of them are floating. [16] has low input impedance and can implement only AP response. [17] can implement only LP and BP responses which are available through passive components, hence requires some more active components (opamps, CC etc.) to use these responses.

Table 1. Comparison of the present work with the previously reported works.

Ref.	No. and type of active components	No. and type of passive components	No. of inputs and input impedance	Possible output responses and output impedance	Simultaneous outputs
[14]	3 CCII	2 floating R 1 grounded R 2 floating C	Single, low input impedance	LP, BP, HP all at high output impedance; NF and AP not possible	3
[15]	3 PFTFN realized using 6 CFOA	2 floating R 1 grounded R 2 floating C	Single, low input impedance	LP, BP, HP all at high output impedance; NF and APF not possible	3
[16]	single CCIII	2 floating R 1 grounded R 1 grounded C	Single, low input impedance	Only AP response at high output impedance	1
[17]	Single opamp	1 floating R 1 grounded R 1 grounded C	Single, high input impedance	LP and BP output Current through passive components; HP, AP, NF not possible	2
[18]	2CDTA	2 floating R 1 floating C 1 grounded C	Three, low input impedance	LP, HP, BP, AP, NF all at high output impedance	1
Present work	3CCCII	2 grounded C	Single, high input impedance	LP, HP, BP, AP, NF all at high output impedance	4 & 3

4) [18] is a good proposition which uses only two active components and implements all responses of universal filter. However, it suffers form the drawback of using excessive numbers of passive components and most of them are floating and also input impedance is low which is not desirable for a transadmittace mode filter.

Hence it reveals that the present work removes most of the drawback which were prevailing in transadmittance mode universal filter reported till date.

4. Simulation Results

To validate the theoretical predictions, the proposed filter is simulated with SPICE using schematic of MOCCCII as given in **Figure 2** [19] using AMS 0.35 μm CMOS technology with dimensions of the NMOS and PMOS transistors as that of [19] and supply voltages of ±1.5 volts. **Figure 5** shows the simulation results for circuit of **Figure 3** with the component values of $C_1 = C_2 = 10$ pF and $I_{01} = I_{02} = 100$ μA. The total power dissipation of the proposed filter is found to be approximately 10 mW.

The simulations have also been carried out to show the dependence of f_0 on bias current and results are shown in **Figure 6** for band pass response. It is found that f_0 depends linearly for low bias currents whereas for higher bias current the dependence is approximately proportional to the square root of the bias current. The percentage total harmonic distortion (%THD) variation with the sinusoidal input signal is also studied and the results are shown in **Figure 7**. It shows that the %THD is low and remains within the acceptable limit of 5% [21] till the considerable high input signal of 800 mV.

5. Conclusions

Two new single-input mutiple-output transadmittance mode universal filters using three MOCCCII and two grounded capacitors have been presented. The simulation results verify the theory. It is found from the comparison that the present work removes most of the drawback of the previously reported works [14-18]. The salient features of the proposed circuits are as follows: use of only three MOCCCIIs and two capacitors, uses grounded passive components, low sensitivity performance, orthogonal and electronic tunability of ω_0 and Q_0, high input and output impedances which ease cascadability and low component spread for high Q application.

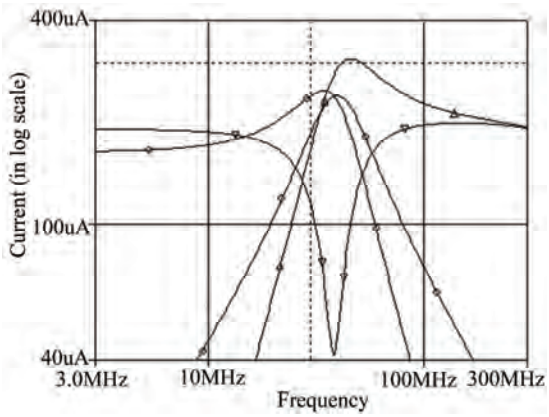

Figure 5. Simulated results for low pass, band pass, high pass and notch responses.

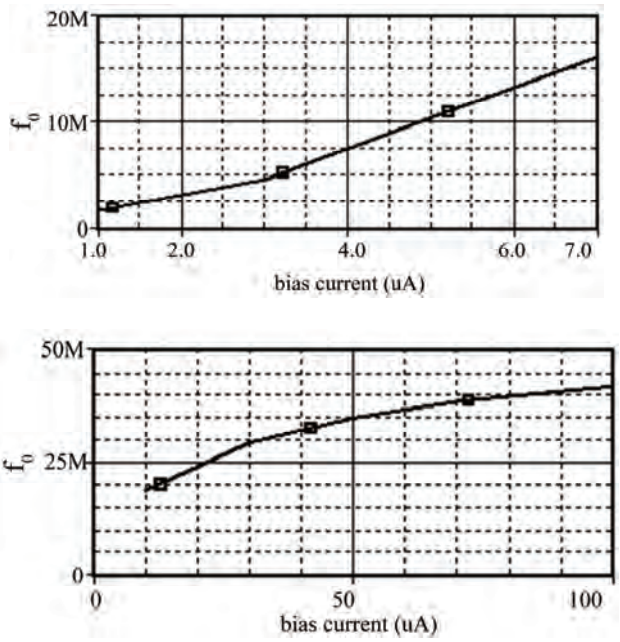

Figure 6. Dependence of central frequency on bias current.

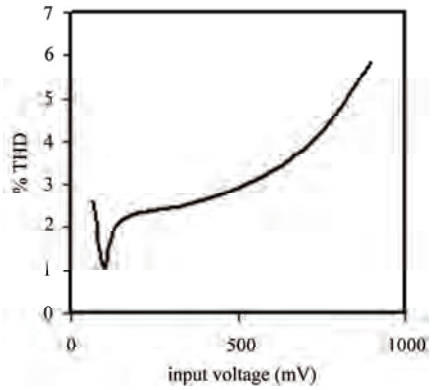

Figure 7. Variation of THD with input signal amplitude.

6. References

[1] G. Ferri and N. C. Guerrini, "Low-Voltage Low-Power CMOS Current Conveyors," Kluwer Academic Publishers, London, 2003.

[2] N. A. Shah, M. F. Rather and S. Z. Iqbal, "Multifunction Mixed Mode Filter Using FTFN," *Analog Integrated Circuits and Signal Processing*, Vol. 47, No. 3, 2006, pp. 339-343.

[3] A. Fabre, O. Saaid, F. Wiest and C. Boucheron, "High Frequency Applications Based on a New Current Controlled Conveyor," *IEEE Transactions on Circuits Systems-I*, Vol. 43, No. 2, 1996, pp. 82-91.

[4] N. Pandey, S. K. Paul and S. B. Jain, "A New Electronically Tunable Current Mode Universal Filter Using MO-CCCII," *Analog Integrated Circuits and Signal Processing*, Vol. 58, No. 2, 2009, pp. 171-178.

[5] S. Ozoguz, A. Toker and O. Cicekoglu, "New Current-Mode Universal Filters Using Only CCII + s," *Microelectronics Journal*, Vol. 30, No. 3, 1999, pp. 255-258.

[6] W. Tangsrirat, "Current Tunable Current Mode Multifunction Filter Based on Dual Output Current Controlled Conveyors," *AEU International Journal of Electronics and Communications*, Vol. 61, No. 8, 2007, pp. 528-533.

[7] J. W. Horng, C. L. Hou, C. M. Chang and W. Y. Chung, "Voltage Mode Universal Biquadratic Filters with One Input and Five Outputs," *Analog Integrated Circuits and Signal Processing*, Vol. 47, No. 1, 2006, pp. 73-83.

[8] O. Cicekoglu and H. Kuntman, "A New Four Terminal Floating Nullor Base Single-Input Three-Output Current-Mode Multifunction Filter," *Microelectronics Journal*, Vol. 30, No. 2, 1999, pp. 115-118.

[9] D. R. Bhaskar, V. K. Sharma, M. Monis and S. M. I. Rizvi, "New Current Mode Universal Biquad Filter," *Microelectronics Journal*, Vol. 30, No. 9, 1999, pp. 837-839.

[10] A. Fabre and M. Alami, "Universal Current Mode Biquad Implemented from Two Second Generation Current Conveyors," *IEEE Transactions on Circuits Systems-I*, Vol. 42, No. 7, 1995, pp. 383-385.

[11] A. Fabre, F. Dayoub, L. Duruisseau and M. Kamoun, "High Input Impedance Insensitive Second-Order Filters Implemented from Current Conveyors," *IEEE Transactions on Circuits Systems-I*, Vol. 41, No. 12, 1994, pp. 918-921.

[12] I. A. Khan and M. H. Zaidi, "Multifunction Translinear-C Current Mode Filter," *International Journal of Electronics*, Vol. 87, No. 6, 2000, pp. 1047-1051.

[13] S. Maheshwari and I. A. Khan, "Novel Cascadable Current-Mode Translinear-C Universal Filter," *Active and Passive Electronic Components*, Vol. 27, No. 4, 2004, pp. 215-218.

[14] A. Toker, O. Cicekoglu, S. Ozacan and H. Kuntman, "High Output Impedance Transadmittance Type Continuous Time Multifunction Filter with Minimum Active Elements," *International Journal of Electronics*, Vol. 88, No. 10, 2001, pp. 1085-1091.

[15] N. A. Shah, S. Z. Iqbal and B. Parveen, "SITO High Output Impedance Transadmittance Filter Using FTFNs," *Analog Integrated Circuits and Signal Processing*, Vol. 40, No. 4, 2004, pp. 87-89.

[16] U. Cam, "A New Transadmittance Type First-Order All Pass Filter Employing Single Third Generation Current Conveyor," *Analog Integrated Circuits and Signal Processing*, Vol. 43, No. 1, 2005, pp. 97-99.

[17] N. A. Shah, S. Z. Iqbal and B. Parveen, "Lowpass and Bandpass Transadmittance Filter Using Operational Amplifier Pole," *AEU International Journal of Electronics and Communications*, Vol. 59, No. 7, 2005, pp. 410-412.

[18] N. A. Shah, M. Quadri and S. Z. Iqbal, "CDTA Based Universal Transadmittance Filter," *Analog Integrated Circuits and Signal Processing*, Vol. 52, No. 1-2, 2007, pp. 65-69.

[19] E. Altuntas and A. Toker, "Realization of Voltage and Current Mode KHN Biquad Using CCCIIs," *AEU International Journal of Electronics and Communications*, Vol. 56, No. 1, 2002, pp. 45-49.

[20] S. I. Liu, "High Input Impedance Filter with Low Component Spread Using Current Feedback Amplifiers," *Electronics Letters*, Vol. 31, No. 13, 1995, pp. 1042-1043.

[21] E. S. Erdogan, R. O. Topaloglu, H. Kuntman and O. Cicekoglu, "New Current Mode Special Function Continuous-Time Active Filters Employing only OTAs and OPAMPs," *International Journal of Electronics*, Vol. 91, No. 6, 2004, pp. 345-359.

Circuits and Systems, **2010, 1, 59-64**
doi:10.4236/cs.2010.12010 Published Online October 2010 (http://www.SciRP.org/journal/cs)

Pulse Skipping Modulated Buck Converter - Modeling and Simulation

Ramamurthy Srinivasan, Vanaja Ranjan P.
Department of EEE, College of Engineering, Guindy, Anna University, Chennai, India
E-mail: *sramamurthy@ieee.org*
Received August 23, 2010; *revised September* 19, 2010; *accepted September* 25, 2010

Abstract

Modeling and simulation results of a pulse skipping modulated buck converter for applications involving a source with widely varying voltage conditions with loads requiring constant voltage from full load down to no load is presented. The pulses applied to the switch are blocked or released on output voltage crossing a predetermined value. The regulator worked satisfactorily over a wide input voltage range with good transient response but with higher ripple content. Input current spectrum indicates a good EMI performance with crowding of components at audio frequency range for the selected switching frequency.

Keywords: DC/DC Converter, Pulse Skipping Modulation, Buck Regulator, Modulation Factor, Electromagnetic Interference

1. Introduction

DC-to-DC buck converters are direct converters employed for stepping down DC voltage to a desired lower level. These are employed, due to their inherent high efficiency, in places where losses due to their linear counterparts are not tolerated. A buck regulator is a suitably controlled buck converter that can maintain its output voltage at the desired level during constant load with varying input voltage conditions, constant input voltage with varying load conditions or both. A voltage mode PWM controller, in which the duty cycle is altered, based on error between set voltage and measured output voltage such that the output voltage of the converter is very nearly equal to the desired value is well documented and widely used [1-4]. These converters are mostly based on circuits in which a pulse width modulated (PWM) signal is filtered with an LC network [5-7]. Apart from maintaining the line and load regulations low, it is also desirable to retain the losses low especially in applications involving energy limited sources. It is required that the efficiency is kept high throughout the operating range. Efficiency of PWM switching regulators is in general high compared to linear regulators but not constant over the entire load range. Efficiency of a PWM regulator at light loads is significantly less compared to that at near full load conditions. The problem is pronounced at low voltage portable applications. Various topologies and methods of control were suggested and synchronous buck topology with ZVS technique is suggested for minimizing switching losses [8-10]. The low side MOSFET device with integrated Schottky diode can further improve the efficiency of synchronous converter even though there is slight increase in ON resistance [11].

The converter, which operates with high efficiency at light loads during stand by mode, in which portable equipment operate most of the time when not in use, demanded considerable attention of the researchers and several techniques including improved controllers with digital PWM, PFM with reduced switching and conduction losses were proposed [12-14]. Pulse Skipping Modulated Converters operate with higher efficiency at light loads with reduced switching loss due to pulse skipping [15]. A pulse skipping modulated DC-DC converter is studied in this paper for its performance under varied supply and load conditions.

2. Pulse Skipping Modulated Buck Converter

2.1. Description

A pulse skipping modulated buck converter is shown in **Figure 1**. It essentially consists of a MOSFET switch, a diode, an inductor L, a capacitor C. L and C filter out the ripple and designed suitably so that the LC filter cut off

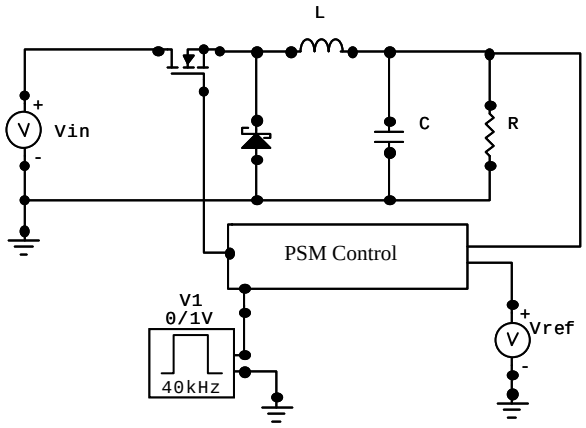

Figure 1. Pulse skipping modulated buck converter.

frequency is well below the switching frequency. The feedback circuit consists of a PSM control logic, which allows the pulse generated by the clock if actual voltage is below the reference voltage and skips pulses if the actual voltage exceeds the reference voltage vref. The clock pulse generated is a constant frequency constant width (CFCW) pulse [16]. MOSFET switch is ON when the clock pulse is applied over a fixed duration of time equal to duty cycle of the clock and the inductor current rises linearly. The switch is OFF for the remaining period of the cycle and the current drops to a lower value but higher than the initial value of the cycle. It drops to a value lower than the initial value if the next pulse is skipped and so on. Thus by alternately permitting p pulses and skipping q pulses the output voltage is maintained at a value close to reference value. The waveforms are shown in **Figure 2**.

As shown in **Figure 3**, a comparator compares v0 and vref and its output is ANDed with CLK. Output of AND gate sets RS flip flop which is reset at the falling edge of the clock as shown through a NOT gate. Pulse Output of the flip-flop is used to drive the converter switch. On vref > v0 comparator output is HIGH and AND gate output sets flip flop every time CLK goes HIGH and is reset at the falling edge. Hence clock pulses are applied

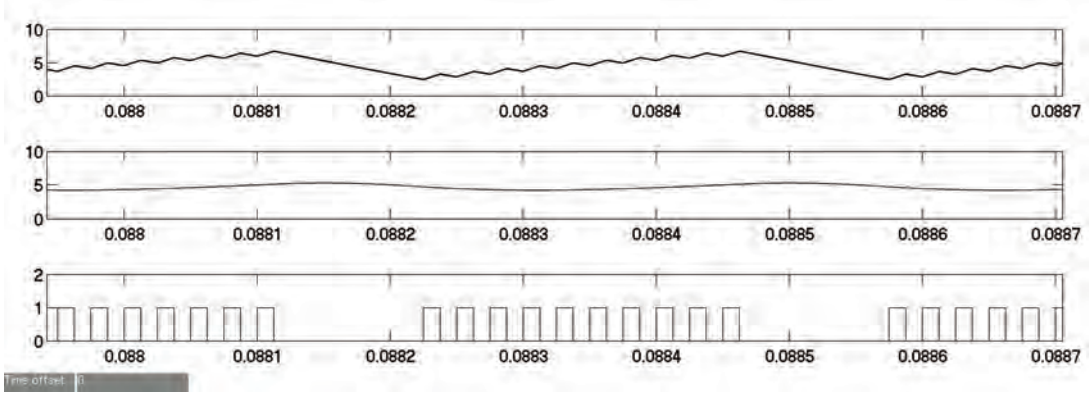

Figure 2. Waveforms of output voltage, Inductor current and gate pulses for a PSM converter.

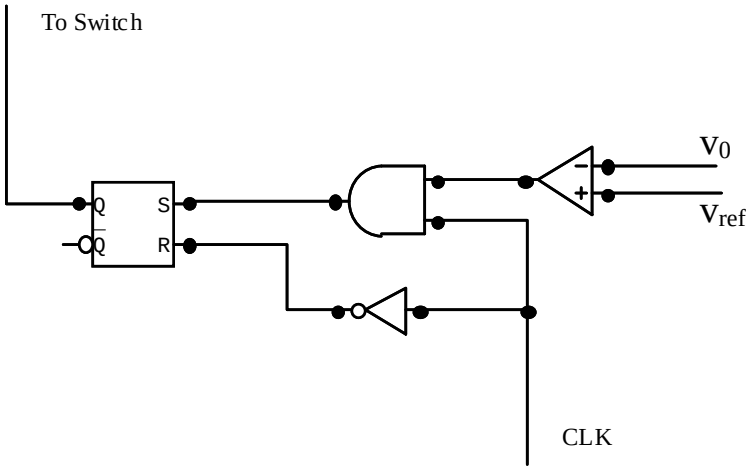

Figure 3. PSM control logic.

to the switch. This is known as charging period. On vrefd < v0 comparator output is LOW and AND gate out put is LOW irrespective of the clock and hence the flip flop is not set and clock pulses are not applied to the switch or pulses are skipped. This is known as skipping period.

3. Modeling of PSM converter

Let for p cycles the clock pulses are applied and for q cycles the pulses are skipped for a particular load resistance R and input voltage Vin. The duration pT is known as charging period and the duration qT is known as skip ping period. During the charging period, in each cycle the switch is ON for duration equal to *D* and during the skipping period the switch is OFF throughout as the pulses are not applied and skipped.

The converter is modeled [16] using state space averaging method and the state space equations, assuming continuous conduction mode, are obtained as shown below.

During charging period,

$$\begin{aligned} \dot{x} &= A_1 x + B_1 v_{in} \qquad 0 \le t \le DT \\ y &= C_1 x \end{aligned} \tag{1}$$

$$\begin{aligned} \dot{x} &= A_2 x + B_2 v_{in} \qquad DT \le t \le T \\ y &= C_2 x \end{aligned} \tag{2}$$

During skipping period,

$$\begin{aligned} \dot{x} &= A_2 x + B_2 v_{in} \qquad 0 \le t \le T \\ y &= C_2 x \end{aligned} \tag{3}$$

where,

$$A_1 = A_2 = A = \begin{bmatrix} 0 & \dfrac{-1}{L} \\ \dfrac{1}{C} & \dfrac{-1}{RC} \end{bmatrix}, \; x = \begin{bmatrix} i_L \\ v_C \end{bmatrix}, \; y = v_0,$$

$$B_1 = \begin{bmatrix} \dfrac{1}{L} \\ 0 \end{bmatrix}, \quad B_2 = 0 \quad C = \begin{bmatrix} 0 & 1 \end{bmatrix}$$

After State Space Averaging,

$$\dot{x} = Ax + \frac{p}{p+q} BDv_{in} \tag{4}$$

Defining Modulation Factor *M*,

$$M = \frac{q}{p+q}$$

Then Equation (4) becomes

$$\dot{x} = Ax + (1-M)DBv_{in} \tag{5}$$

Hence the average output voltage is given by

$$V_0 = (1-M)Dv_{in} \tag{6}$$

M, the modulation factor is a measure of the number of skipping. When vin goes higher for the same V_0 with constant *D*, *M* increases increasing the number of skipped pulses to maintain the voltage. Similarly when load decreases *M* increases decreasing the number of switching. When no pulses are skipped then *M* is zero and the equation reduces to that of a buck converter without feedback at steady state.

4. Simulation

Simulation of the PSM DC-DC buck converter was carried out with the following parameters. v_{in} = 12 V to 20 V, V_0 = 5 V, L = 150 μH, C = 20 μF, f = 40 KHz.

Pulses are skipped to regulate the output voltage with increase in input voltage as shown in **Figure 4**.

Input voltage is stepped from 12 V to 20 V and the output voltage is plotted. Output voltage waveform for a constant load with a step increase in input voltage is shown in **Figure 5**.

Response showed that PSM converter can accept wide variations in input voltage and its response speed was good as seen from step response and the output voltage was regulated over the entire range. Modulation Factor increases with increase in voltage increasing the pulses skipped Load was decreased by a step and the output voltage is shown in **Figure 6**. Pulses skipped increased, as load was decreased to regulate the voltage. The ripple of the output voltage was higher as input voltage was increased. A similar response was observed when the load was decreased. Input current harmonic spectrum of the PSM converter is shown in **Figure 7**. Spectrum of the converter with PWM control is also shown in **Figure 8** for comparison purpose for the same input voltage and load.

In the case of PSM converter harmonic components are spread over a wide band of frequencies lowering the average value of the peaks of currents. Individual peaks are smaller than those of PWM converter. Hence PSM converter has better EMI performance. Due to reduction in average frequency with pulse skipping at light loads there may be components entering into audio frequency range which may result in audible noise interference, which can be avoided by selecting the switching frequency high.

5. Conclusions

Pulse Skipping Modulated Buck converter was modeled and simulated. Response of the converter for input voltage and load step variation was studied. The converter response to changes was quick and the PSM controlled converter regulated the output voltage over the entire

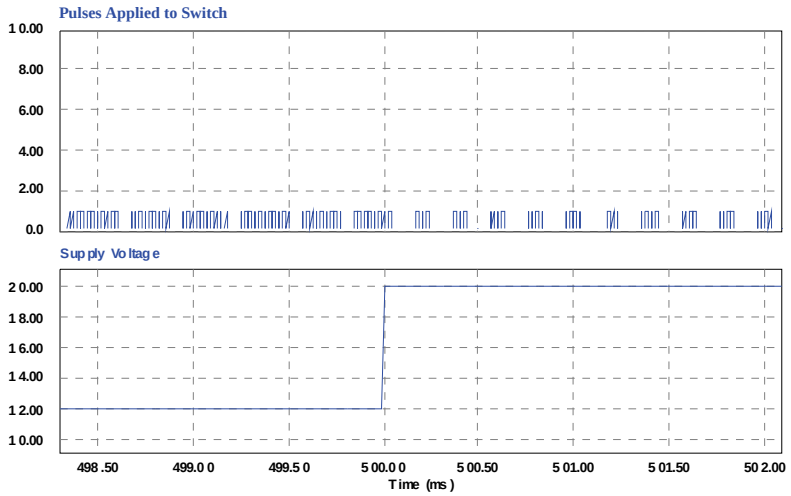

Figure 4. Increased pulse skipping with input voltage increase.

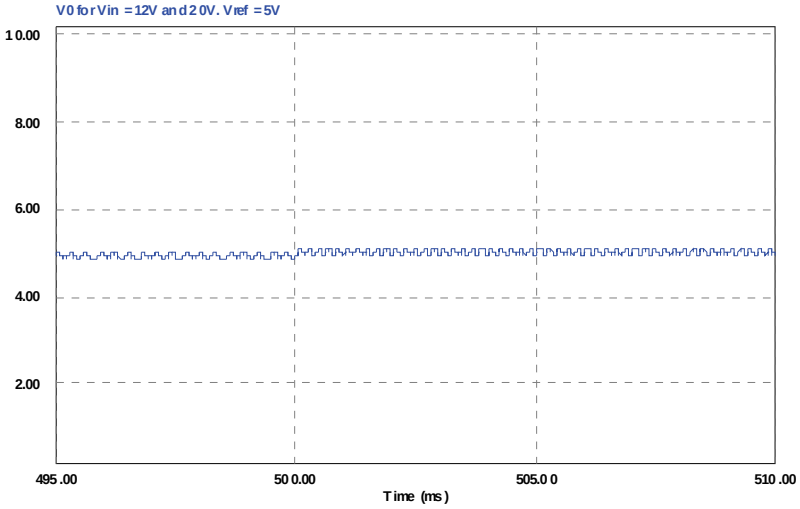

Figure 5. Output voltage for step increase in input voltage.

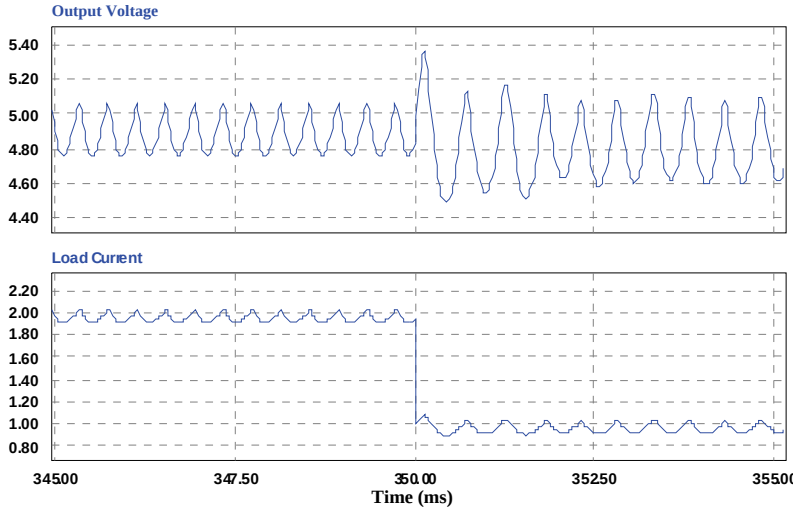

Figure 6. Output voltage for step decrease in load current.

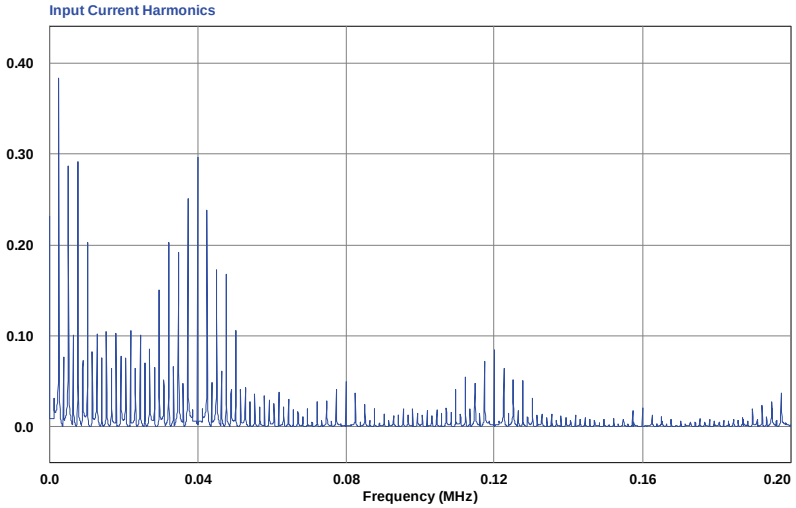

Figure 7. Input current harmonic spectrum – PSM converter.

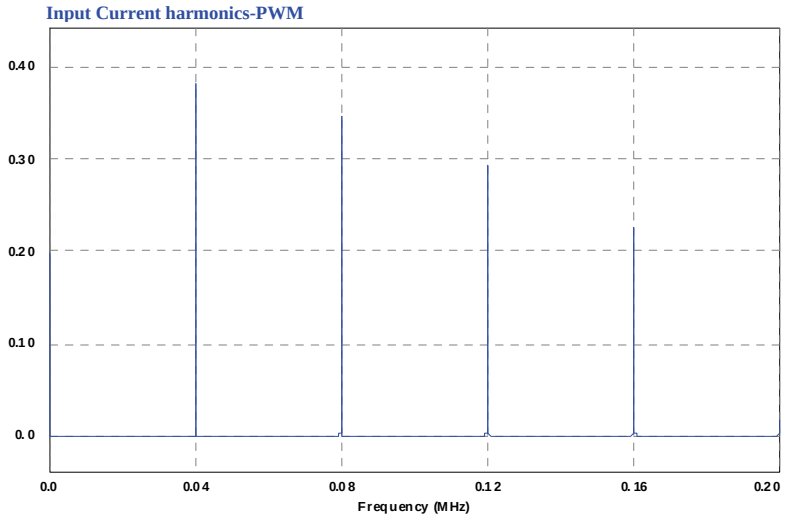

Figure 8. Input current harmonic spectrum – PWM converter.

range of input voltage intended for operation. Input current harmonic spectrum was studied and compared with that of PWM controlled Converter. PSM converter has a well spread out spectrum, with individual component peak values less in amplitude, making its EMI performance better than that of PWM controlled converter. But there are frequency components entering into audio frequency range due to the average frequency of switching being lower with pulse skipping, if the switching frequency is selected to be just above the audio range.

6. References

[1] R. W. Erickson and D. Maksimovic, "Fundamentals of Power Electronics," 2nd Edition, Kluwer Academic Publishers, Dordrecht.

[2] A. J. Forsyth and S. V. Mollow, "Modelling and Control of DC-DC Converters," *IEE Power Engineering Journal*, Vol. 12, No. 5, October 1998, pp. 229-236.

[3] J. G. Kassakian, M. F. Schlecht and G. C. Verghese, "Principles of Power Electronics," Addison-Wesley, Reading, June 1992.

[4] B. Arbetter, R. Erickson and D. Maksimovic, "DC-DC Converter Design for Battery-Operated Systems," *IEEE PESC*'95. Vol. 1, June 1995, pp. 103-109.

[5] A. J. Stratakos, S. R. Sanders and R. W. Broderson, "A Low-Voltage CMOS DC–DC Converter for a Portable Battery-Operated System," *Proceedings of Power Electronics Specialists Conference*, Taiwan, Vol. 1, June 1994, pp. 619-626.

[6] G. Y. Wei and M. Horowitz, "A Fully Digital, Energy-Efficient Adaptive Power-Supply Regulator," *IEEE Journal of Solid-State Circuits*, Vol. 35, April 2000, pp.

520-528.

[7] A. P. Dancy, R. Amirtharajah and A. P. Chandrakasan, "High-Efficiency Multiple-Output DC–DC Conversion for Low-Voltage Systems," *IEEE Transactions on VLSI*, Vol. 8, June 2000, pp. 252-263.

[8] A. V. Peterchev and S. R. Sanders, "Digital Loss – Minimizing Multi-Mode Synchronous Buck Converter Control," 35*th Annual IEEE Power Electronics Specialists Conference*, Vol. 6, Aachen, 2004, pp. 3694-3699.

[9] S. Pattnaik, A. K. Panda, K. Aroul and K. K. Mahapatra, "A Novel Zero Voltage Transition Synchronous Buck Converter for Portable Application," *International Journal of Electrical, Computer, and Systems Engineering*, Vol. 2, No. 2, 2008, pp. 115-120.

[10] A. Consoli, F. Gennaro, C. Cavallaro and A. Testa, "A Comparative Study of Different Buck Topologies for High-Efficiency Low-Voltage Applications," *Proceedings on Power Power Electronics Specialist Conference*, 1999, pp. 60-65.

[11] D. Calafut, "Trench Power MOSFET Lowside Switch with Optimized Integrated Schottky Diode," *Proceedings of the* 16*th International Symposium on Power Semiconductor Devices and ICs* (*ISPSD*'04), 24-27 May 2004, pp. 397-400.

[12] K. M. Smith and K. M. Smedly, "A Comparison of Voltage-Mode Soft Switching Methods for PWM Converters," *IEEE Transactions on Power Electronics*, Vol. 12, No. 2, 1997, pp. 376-386.

[13] X. W. Zhou, M. Donati, L. Amoroso and F. C. Lee, "Improved Light-Load Efficiency for Synchronous Rectifier Voltage Regulator Module," *IEEE Transactions on Power Electronics*, Vol. 15, No. 5, September 2000, pp. 826-834.

[14] C.-L. Chen, W.-L. Hsieh, W.-J. L. K.-H. Chen and C.-S. Wang, "A New PWM/PFM Control Technique for Improving Efficiency over Wide Load Range," 15*th IEEE International Conference on Electronics, Circuits and Systems*, Malta, 2008, pp. 962-965.

[15] P. Luo, L. Y. Luo, Z. J. Li, *et al.*, "Skip Cycle Modulation in Switching DC-DC Converter," *International Conference on Communications, Circuits, and Systems*, Chengdu, June 2002, pp. 1716-1719.

[16] P. Luo, B. Zhang, S.-P. Wang and F. Yong, "Modeling and Analysis of Pulse Skip Modulation," *Journal of Electronic Science and Technology of China* (*Chinese*), Vol. 4, No. 1, March 2006.

[17] A. Farhadi and A. Jalilian, "Modeling, Simulation and Reduction Techniques of Electromagnetic Conducted Emission Due to Operation of Power Electronic Converters," *International Conference on Renewable Energy and Power Quality* (*ICREPQ*'07), Sevilla, March 2007.

[18] F. Lin and D. Y. Chen, "Reduction of Power Supply EMI Emission by Switching Frequency Modulation," *IEEE Transactions on Power Electronics*, Vol. 9, No. 1, January 1994, pp. 132-137.

Circuits and Systems, **2010, 1, 65-70**
doi:10.4236/cs.2010.12011 Published Online October 2010 (http://www.SciRP.org/journal/cs)

Third Order Current Mode Universal Filter Using Only Op.amp. and OTAs

G. N. Shinde[1], D. D. Mulajkar[2]
[1]*Indira Gandhi* (*SR*) *College, Nanded, Maharashtra, India*
[2]*Dnyanasadhana College, Thane, Maharashtra, India*
E-mail: *shindegn@yahoo.co.in*
Received August 5, 2010; *revised September* 8, 2010; *accepted September* 15, 2010

Abstract

A novel current mode active-only universal filter using four dual current output Operational Transconductance Amplifiers (OTAs) and three Operational Amplifiers (OAs) is presented. The circuit can realize low pass and high pass filter characteristics by choosing the suitable current output branches. The filter performance factors natural frequency (ω_0), bandwidth $(\frac{\omega_0}{Q})$, quality factor Q and transconductance gain gm are electronically tunable. The proposed circuit has very low sensitivities with respect to circuit active elements. From sensitivity analysis, it has been clearly shown that the proposed circuit has very low sensitivities with respect to the circuit active elements. The gain roll-off of high pass and low pass configuration is 18 dB/octave. The proposed circuit facilitates integrability, programmability and ease of implementation.

Keywords: Current Mode Filter, OTA, Bandwidth, Center Frequency, Circuit Merit Factor Q

1. Introduction

In recent years, current mode analogue signal processing circuit techniques have received wide attention due to the high accuracy, the wide signal bandwidth and the simplicity of implementing signal operations [1]. The design of current mode circuits employing active devices such as OAs, OTAs, and current conveyors (CCs) have been reported in the literature [2-6]. An OTA provides a high linear electronic tunability and wide tunable range of its transconductance gain.OTA based circuits requires no resistors; hence they are suitable for monolithic integration.

Recently, the multiple current output OTAs have been used for realizing current mode filters [7-12]. In 1996, Tsukutani *et al*. proposed good versatile current mode biquad filter using multiple current output OTAs and two grounded capacitors.

This paper focuses on realization of the current-mode third order active-only filter. The proposed circuit is constructed with OAs and dual current output OTAs. It is shown that the circuit can realize the biquadratic transfer function, and that the circuit characteristics can be electronically tuned by the transconductance gains of OTAs. The proposed circuit enjoys the features of:

- saving in components,
- realization of various filtering responses,
- devoid of resistors and capacitors which suits IC design techniques,
- high impedance outputs,
- electronic adjustment of ω_0 and $\frac{\omega_0}{Q}$ through bias currents of the active elements
- independent electronic adjustment of passband gains,
- low sensitivity figures.

2. Circuit Analysis and Analytical Treatment

The open loop gain of an OA is represented by the well known first order pole model [13-15]

$$A(S) = \frac{A_0\omega_0}{S+\omega_0}$$

where $A_{0:}$ Open loop D.C. gain of op-amp.

ω_0 : Open loop – 3dB bandwidth of the op-amp = 2 пf$_0$

$A_0\,\omega_0 : \beta_i$ = gain-bandwidth product of op-amp.

For $S >> \omega_0$

$$A(S) = \frac{A_0\omega_0}{S} = \frac{\beta_1}{S} \qquad (i = 1,2,3,)$$

This model of OA is valid from a few kHz to few hundred kHz. In this frequency range, OTA works as an ideal device. The OTA is characterized by the port-relation

$$I_O = g_m (V_+ - V_-)$$

where, g_m is transconductance of OTA. In the dual current output OTA, the plus current output has a positive polarity, and the minus current output has a negative polarity.

The analysis gives the current transfer function T = [*I out / I in*] as follows:

$$T(S) = \frac{g_{mb0}S^3 - (g_{mb1}\beta_1 - g_{mb2}\beta_2)S^2 + (g_{mb2}\beta_1\beta_2 - g_{mb3}\beta_2\beta_3)S - g_{mb3}\beta_1\beta_2\beta_3}{g_{ma0}S^3 + (g_{ma1}\beta_1 - g_{ma2}\beta_2)S^2 + (g_{ma2}\beta_1\beta_2 + g_{ma3}\beta_2\beta_3)S + g_{ma3}\beta_1\beta_2\beta_3} \quad (1)$$

The circuit was designed using coefficient matching technique. *i.e.*, by comparing these transfer functions with general third order transfer functions is given by,

$$T(S) = \frac{\alpha_3 S^3 + \alpha_2 S^2 + \alpha_1 S + \alpha_0}{S^3 + \omega_0(1+\frac{1}{Q})S^2 + \omega_0^2(1+\frac{1}{Q})S + \omega_0^2} \quad (2)$$

Comparing Equations (1) with (2) we get,

$$\omega_0^3 = \frac{g_{ma3}\beta_1\beta_2\beta_3}{g_{ma0}} \quad \omega_0^2(1+\frac{1}{Q}) = \frac{g_{ma1}\beta_1 + g_{ma2}\beta_2}{g_{ma0}} \quad (3)$$

$$\omega_0(1+\frac{1}{Q}) = \frac{g_{mb2}\beta_1\beta_2 + g_{mb3}\beta_2\beta_3}{g_{ma0}}$$

$$\alpha_3 = \frac{g_{mb0}}{g_{ma0}} \text{ And } \alpha_0 = \frac{g_{mb3}}{g_{ma0}}$$

It is found from above equations that circuit parameters ω_0, Q; α_0 can independently set and electronically tuned adjusting the transconductance gains of the OTAs. If g_{ma0}, β_1, β_2 and β_3 are given, the parameter ω_0 can be set by g_{ma2}. The parameters Q and α_3 can be set by g_{ma1} and g_{mb0} respectively. It seems that the values of Q and α_3 are also limited by the dynamic ranges of the OA and OTA.

From (1), it can be seen that:

1) The low pass transfer function can be realized with $g_{mb0} = 0$

$g_{mb1}\beta_1 = g_{mb2}\beta_2$ and $g_{mb2}\beta_1\beta_2 = g_{mb3}\beta_2\beta_3$

2) The high pass transfer function can be realized with $g_{mb3} = 0$ $g_{mb1}\beta_1 = g_{mb2}\beta_2$ and $g_{mb2}\beta_1\beta_2 = g_{mb3}\beta_2\beta_3$

3) The band pass transfer function can be realized with $g_{mb3} = g_{mb0} = 0$ $g_{mb1}\beta_1 = g_{mb2}\beta_2$

The high pass and low pass transfer functions obtained are as follows,

$$T_{HP} = \frac{\alpha_0 S^3}{g_{ma0}S^3 + (g_{ma1}\beta_1 + g_{ma2}\beta_2)S^2 + (g_{ma2}\beta_1\beta_2 + g_{ma3}\beta_2\beta_3)S + g_{ma3}\beta_1\beta_2\beta_3}$$

$$T_{LP} = \frac{\alpha_3}{g_{ma0}S^3 + (g_{ma1}\beta_1 + g_{ma2}\beta_2)S^2 + (g_{ma2}\beta_1\beta_2 + g_{ma3}\beta_2\beta_3)S + g_{ma3}\beta_1\beta_2\beta_3}$$

The realization of the other transfer functions invariably requires matching the conditions in terms of the transconductance gains of the OTAs and the gain-bandwidth products of the OAs.

The transconductance gains of the OTAs to realize the desired characteristics are obtained from (3) as

$$g_{ma3} = \frac{\omega_0^3\beta_1\beta_2\beta_3}{g_{ma0}}$$

$$g_{ma2} = \frac{\omega_0^2}{\beta_1\beta_2}\{\left(1+\frac{1}{Q}\right) - \frac{g_{ma0}\omega_0}{\beta_1\beta_2\beta_3}\}$$

$$g_{ma1} = \frac{g_{ma0}\omega_0}{\beta_1}\left(1+\frac{1}{Q}\right) - \frac{g_{ma2}\beta_2}{\beta_1}$$

where ω_0, Q, β_1, β_2, β_3 and g_{ma0} should be given in advance.

Methods of implementing a dual current output OTA have been discussed previously (Ramirez-Angulo *et al*. 1992, Wu 1994).

3. Circuit Diagram

The diagram was shown in **Figure 1**.

4. Circuit Description

The proposed circuit is built with four dual current output OTAs and three OAs is as shown in **Figure (1)**. The V+ terminal of first OTA and V-terminal of all other OTAs are grounded. Output terminal of first OTA carrying positive polarity current is fed to inverting terminal of first OA. Its output is fed to inverting terminal of

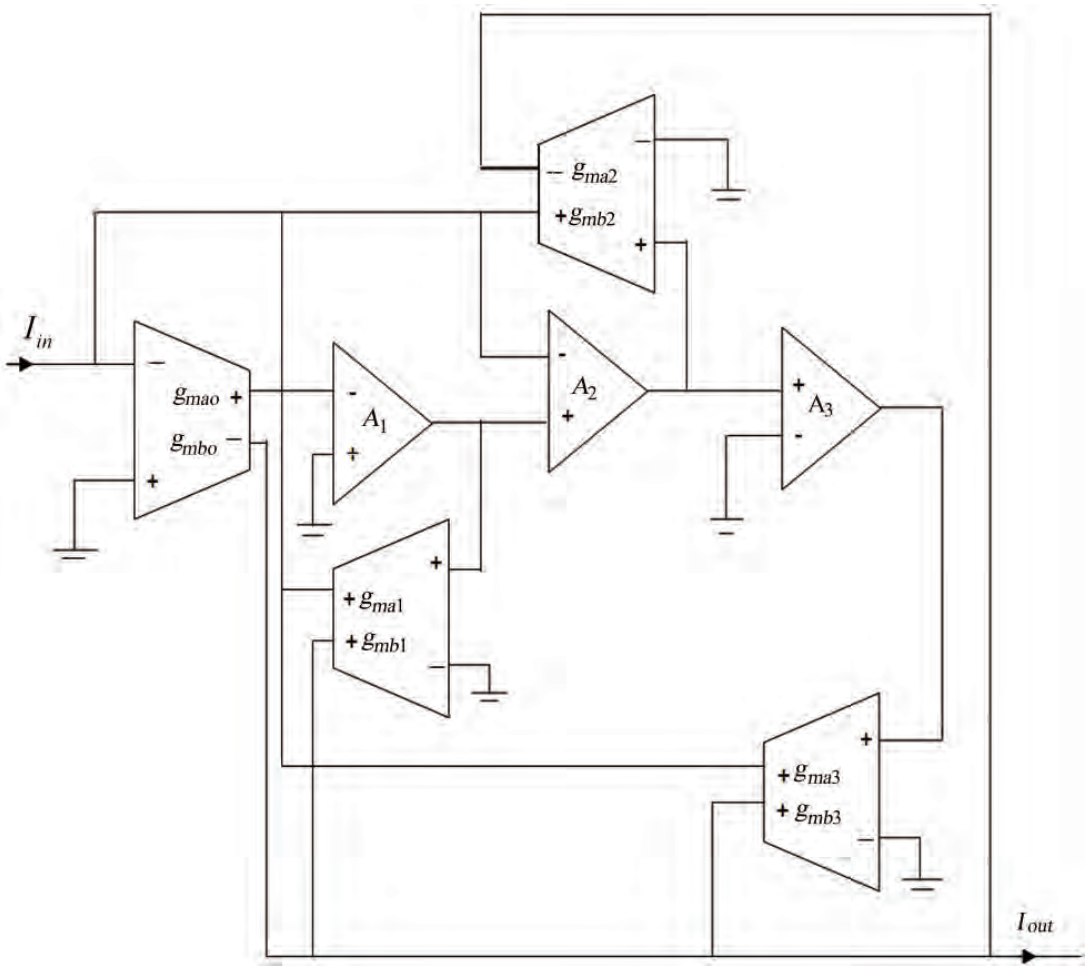

Figure 1. Circuit diagram of electronically tunable third order current-mode universal filter.

non-inverting of third OA output of third OA is then fed to v+ terminal fourth OTA. Output terminals of all OTAs carrying positive current are fed to inverting of first OA whereas remaining current output terminals of all OTAs adds to give output current of the circuit. The circuit can realize various third order filter functions by suitably choosing the current output branches.

5. Result and Discussion

The circuit performance is studied for Central frequencies f_0 = 100 kHz and 1 MHz with circuit merit factor Q = 1. The general operating range of this filter is 10 Hz to 1 MHz. The value of $\beta_1 = \beta_2 = \beta_3 = 6.392 \times 10^6$ for LF 356 N. The proposed circuit gives response only for very high frequencies since the values of transconductance of OTAs takes very low values at frequencies less than 100 kHz. The values of g_{ma1}, g_{ma2} and g_{ma3} are calculated by taking g_{ma0} = 2 and $\frac{g_{ma3}}{g_{ma0}} = 1$ Response is studied for Q = 1 for high pass and low pass function. **Figures 2** and **3** shows high pass and low pass response of the proposed filter circuit respectively. Data obtained after analysis high pass and low pass response is given in **Tables 2** and **3**. From **Figures 2** and **3**, it is seen that the gain roll-off is 18 dB/octave for both the functions and the gain stabilizes to 0 dB at frequency 200Hz. There is no overshoot in the response. Observed - 3 dB frequency *i.e.* cutoff frequency matches with designed value f_0. Thus the filter circuit works ideal for high pass as well as low pass function. The values of transconductance gains for f_0 = 100 kHz and 1 MHz obtained are given in **Tables 1(a)** and **(b)** respectively.

6. Sensitivities

The practical solution is to design a network that has low sensitivity to element changes [14,15]. Thus sensitivity must be less than limit *i.e.* unity. The lower the sensitivity of the circuit, the less will its performance deviate because of element changes. The sensitivities $S_x^{\omega_0}$ and

$S_x^{\alpha_3}$ with respect to the circuit active elements are shown in **Table 4**. These values are within the range $0 \le S_x^y \le 1$ It is found that the proposed circuit has very low sensitivity with respective to active elements.

7. Concluding Remarks

A versatile current-mode active-only filter using OAs and OTAs has been proposed. The proposed circuit can

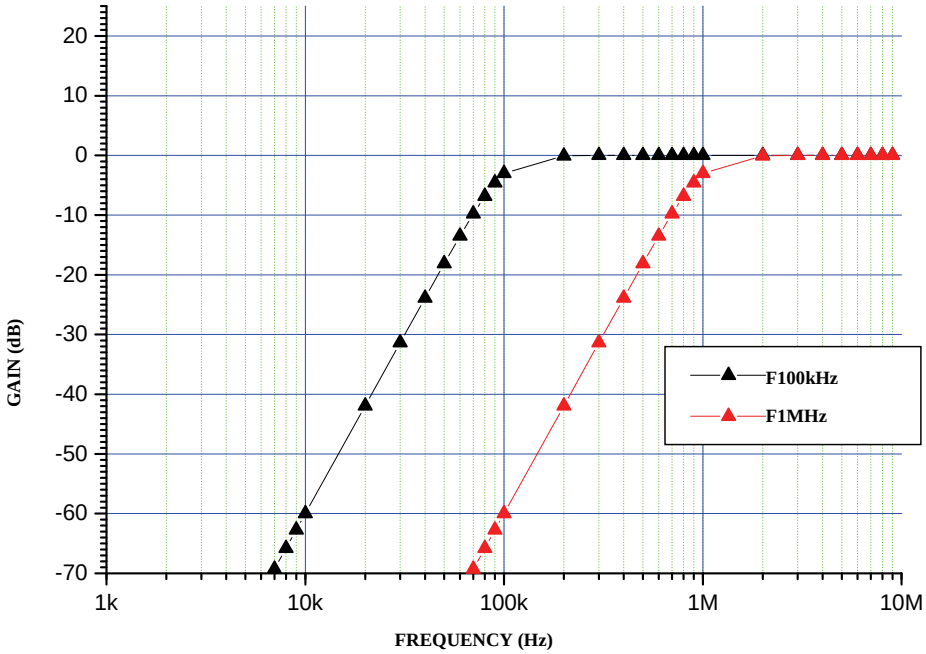

Figure 2. High pass response of proposed current-mode filter.

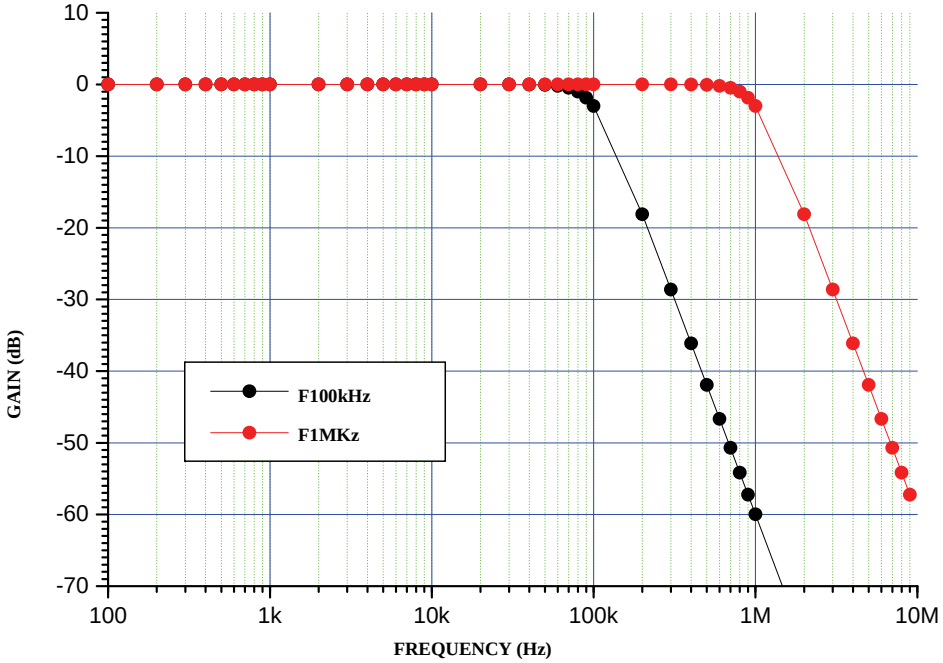

Figure 3. Low pass response of proposed current-mode filter.

Table 1. The values of transconductance gains.

g_{ma}	Value in mS for f_0 = 100 kHz
g_{ma0}	2
g_{ma1}	0.356
g_{ma2}	0.0367
g_{ma3}	0.0019
g_{mb0}	2
g_{mb3}	0.0019

(a) for f_0 = 100 kHz

g_{ma}	Value in mS for f_0 = MHz
g_{ma0}	2
g_{ma1}	1.966
g_{ma2}	1.965
g_{ma3}	1.9
g_{mb0}	2
g_{mb3}	1.9

(b) for f_0 = 1 MHz

Table 2. Analysis of frequency response of high pass function for Q = 1.

f_0 (kHz)	F_{OH} (kHz)	$f_0 \sim F_{OH}$ (kHz)	Gain Roll-off in stop band		Gain Stabilization	
			dB/Octave	Octave starting at (kHz)	dB	F_S (kHz)
100	100	0	18	500	0	
1 M	1 M	0	18	500	0	2 M

F_{OH}: –3 dB Frequency F_S: Frequency at which gain stabilizes

Table 3. Analysis of frequency response of low pass function for Q = 1.

f_0 (kHz)	F_{OL} (kHz)	$f_0 \sim F_{OL}$ (kHz)	Gain Roll-off in stopband		Gain Stabilization	
			dB/Octave	Octave starting at (kHz)	dB	F_S (Hz)
100	100	0	18	400	0	100
1M	1M	0	18.3	2 M	0	100

F_{OL}: –3 dB Frequency

realize the biquadratic transfer function and the circuit characteristics can be electronically tuned by the transconductance gains. From sensitivity analysis, it has been clearly shown that the proposed circuit has very low sensitivities with respect to the circuit active elements.

Table 4. Sensitivities $S_x^{\omega_0}$ and $S_x^{\alpha_3}$.

x	$S_x^{\omega_0}$	$S_x^{\alpha_3}$
g_{ma0}	–0.33	–1.0
g_{ma1}	0	0
g_{ma2}	0	0
g_{ma3}	0.33	0
g_{mb0}	0.33	1.0
β_1	0.33	0
β_2	0.33	0
β_3	0.33	0

The gain roll-off of high pass and low pass configuration is 18dB/octave.

8. References

[1] T. Tsutani, T. Higashimura, Y. Sumi and Y. Fukui, "Electonically Tunable Current Mode Active Only Biquadratic Filter," *International Journal of Electronics*, Vol. 87, No. 3, 2000, pp. 307-314.

[2] C.-C. Hsu and W.-S. Feng, "Dynamic Decoupling and Compensating Methods of Multi-Axis Force Sensors," *International Journal of Electronics*, Vol. 88, No. 1, 2001, pp. 41-51.

[3] I. A. Khan and M. H. Zaidi, "Multifunction Translinear-C Current – Mode Filter," *International Journal of Electonics*, Vol. 87, No. 9, 2000, pp. 1047-1051.

[4] M. Higashimura, "Current Mode Low Pass and Band Pass Filters Using the Operational Amplifier Pole," *International Journal of Electronics*, Vol. 74, No. 6, 1993, pp. 945-949.

[5] T. M. Ishida, Y. Fukui and S. Tsuiki, "Novel Electronically Tunable Current Mode Filter without External Passive Elements," *IEEE*, Vol. 1, 1996, pp. 262-265.

[6] G. W. Roberts and A. S. Sedra, "A General Class of Current Amplifier Based Biquadratic Filter Circuits," *IEEE Transactions on Circuits and Systems*, Vol. 39, No. 4, 1992, pp. 257-263.

[7] J. Ramirez-Angulo, M. Robinson and E. Sanchez-Sinencio, "Current Mode Continuous Time Filters Two Design Approaches," *IEEE Transactions on Circuits and Systems*, Vol. 39, No. 6, 1992, pp. 337-341.

[8] N. A. Shah, M. F. Rather, M. A. Malik and S. Z. Iqbal, "Cascadable Electronically Tunable Sito Current Mode Active Only Universal Filter," *ETRI Journal*, Vol. 26, 2004, pp. 295-300.

[9] A. K. Mitra and V. K. Aatre, "Low Sensitivity High-Frequency Active R Filters," *I.E.E.E. Transactions on Circuits and Systems*, Vol. 23, No. 11, 1976, pp. 670-676.

[10] G. N. Shinde and P. B. Patil, "Sadhana," *Journal of Engineering Science*, Vol. 28, No. 6, 2003, pp. 1919-1926.

[11] T. Tsukutani, M. Higashimura, Y. Sumi and Y. Fukui, "Novel Voltage-Mode Biquad Using Only Active Devic-

es," *International Journal of Electronics*, Vol. l87, No. 3, 2000, pp. 307-314.

[12] R. Nandi "Active R Realization of Bilinear RL Impedances and their Applications in a High-Q Parallel Resonator and External Oscillator," *Proceeding of the Institute of Electrical and Electronics Engineering*, Vol. 66, No. 12, 1978, pp. 1666-1668.

[13] G. N. Shinde and D. D. Mulajkar, "Electronically Tunable Current-Mode Second Order High Pass Filter for Different Value of Q," *International Journal of Physical Sciences*, Vol. 3, No. 6, 2008, pp. 148-151.

[14] D. R. Bhaskar, U. R. Sharma and S. M. I. Rizvi, "New Current-Mode Universal Biquadratic Filter," *Microelectronic Journal*, Vol. 88, No. 10, 1999, pp. 837-839.

[15] S. Minaei and S. Turkoz, "Current-Mode Electronically Tunable Universal Filter Using Only Plus-Type Current Controlled Conveyors and Grounded Capacitors, Bandpass High Pass Filter," *ETRL Journal*, Vol. 26, No. 4, 2004, pp. 292-296.

Circuits and Systems, **2010, 1, 71-75**
doi:10.4236/cs.2010.12012 Published Online October 2010 (http://www.SciRP.org/journal/cs)

New Communication Bands Generated by Using a Soliton Pulse within a Resonator System

P. P. Yupapin[1], M. A. Jalil[2,3], I. S. Amiri[3], I. Naim[3], J. Ali[3]
[1]*Advanced Research Center for Photonics, Faculty of Science King Mongkut's Institute of Technology Ladkrabang, Bangkok, Thailand*
[2]*Ibnu Sina Institute for Fundamental Science Studies, Universiti Teknologi Malaysia, Johor Bahru, Malaysia*
[3]*Institute of Advanced Photonics Science, Nanotechnology Research Alliance, Universiti Teknologi Malaysia, Johor Bahru, Malaysia*
E-mail: *kypreech@kmitl.ac.th*
Received August 5, 2010; *revised September* 8, 2010; *accepted September* 15, 2010

Abstract

We propose a novel system of a broadband source generation using a common soliton pulse (*i.e.* with center wavelength at 1.55 μm) propagating within a nonlinear microring and nanoring resonators system. A system consists of a micro ring resonator system incorporating an add/drop filter, whereas the large bandwidth signals can be generated, stored and regenerated within the system. By using the appropriate parameters relating to the practical device such as micro ring radii, coupling coefficients, linear and nonlinear refractive index, we found that the obtained multi soliton pulses have shown the potential of application for dense wavelength division application, whereas the different center wavelengths of the soliton bands can be obtained via the add/drop filter, which can be used to increase the channel capacity in communication network.

Keywords: Ring Resonator, Photonic Device, Optical Waveguide

1. Introduction

The demand of communication channels and network capacity has been increased significantly for three decades, however, up to now, the large user demand remains. Therefore, the searching of new techniques is needed, which is focused on the communication channel and network capacity. Recently, Pornsuwancharoen *et al.* [1] have reported the very interesting result of the technique that can be used to fulfill the large demand. They have shown that the signal bandwidth can be stretched and compressed by using the nonlinear micro ring system [2-4]. By using such a scheme, the increasing in communication channels using soliton communication is plausible. Furthermore, the long distance communication link is also available. However, several problems are required to solve and address, for instance, the problem of soliton-soliton interaction and collision [5], and the waveguide structure that the broadband soliton can be confined [6]. In this letter, we propose the technique that can be used to generate the new soliton communication bands (wavelength bands), whereas the common soliton pulse, *i.e.*, a soliton source is at the center wavelength of 1.55 m. The soliton bands at the required center wavelengths can be stored [7] and filtered by using the add/drop filter [5]. In application, the use of super dense wavelength multiplexing, with the long distance link is available. Furthermore, the personnel channel and network may be plausible due to the very available bandwidths. However, the problem of the soliton interaction and collision is required to solve, which can be avoided by the specific free spectrum range design [5].

2. Theoretical Background

To maintain the soliton pulse propagating within the ring resonator, the suitable coupling power into the device is required, whereas the interference signal is a minor effect compared to the loss associated to the direct passing through. A soliton pulse, which is introduced into the multi-stage micro ring resonators as shown in **Figure 1**, the input optical field (E_{in}) of the soliton input is given by an Equation (1) [7].

$$E_{in}(t) = A\sec h\left[\frac{T}{T_0}\right]\exp\left[\left(\frac{z}{2L_D}\right) - i\omega_0 t\right] \quad (1)$$

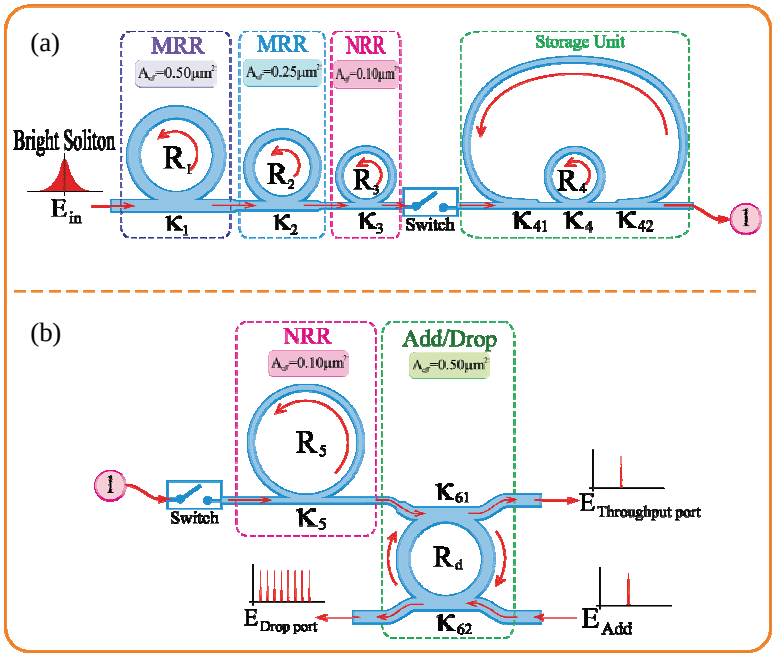

Figure 1. A broadband generation system. (a) a broadband source generation and a storage unit; (b) a soliton band selector, where R_s: ring radii, κ_s: coupling coefficients, κ_{41}, κ_{42}: coupling losses, k_{61} and k_{61} are the add/drop coupling coefficients.

where A and z are the optical field amplitude and propagation distance, respectively. T is a soliton pulse propagation time in a frame moving at the group velocity, $T = t-\beta_1*z$, where β_1 and β_2 are the coefficients of the linear and second order terms of Taylor expansion of the propagation constant. $L_D = T_0^2/|\beta_2|$ is the dispersion length of the soliton pulse. T_o in equation is a soliton pulse propagation time at initial input. Where t is the soliton phase shift time, and he frequency shift of the soliton is ω_0. This solution describes a pulse that keeps its temporal width invariance as it propagates, and thus is called a temporal soliton. When a soliton peak intensity $\left(|\beta_2/\Gamma T_0^2|\right)$ is given, then T_o is known. For the soliton pulse in the micro ring device, a balance should be achieved between the dispersion length (L_D) and the nonlinear length ($L_{NL} = (1/\Gamma\phi_{NL})$, where $\Gamma = n_2*k_0$, is the length scale over which dispersive or nonlinear effects makes the beam becomes wider or narrower. For a soliton pulse, there is a balance between dispersion and nonlinear lengths, hence $L_D = L_{NL}$.

When light propagates within the nonlinear material (medium), the refractive index (n) of light within the medium is given by

$$n = n_0 + n_2 I = n_0 + (\frac{n_2}{A_{eff}})P, \qquad (2)$$

where n_0 and n_2 are the linear and nonlinear refractive indexes, respectively. I and P are the optical intensity and optical power, respectively. The effective mode core area of the device is given by A_{eff}. For the micro ring and nano ring resonators, the effective mode core areas range from 0.50 to 0.1 μm^2 [8], where they found that fast light pulse can be slow down experimentally after input into the nano ring.

When a soliton pulse is input and propagated within a micro ring resonator as shown in **Figures 1(a)** and **(b)**, which consists of a series micro ring resonators. The resonant output is formed, thus, the normalized output of the light field is the ratio between the output and input fields ($E_{out}(t)$ and $E_{in}(t)$) in each roundtrip, which can be expressed as

$$\left|\frac{E_{out}(t)}{E_{in}(t)}\right|^2 = (1-\gamma)\left[1-\frac{(1-(1-\gamma)x^2)\kappa}{(1-x\sqrt{1-\gamma}\sqrt{1-\kappa})^2+4x\sqrt{1-\gamma}\sqrt{1-\kappa}\sin^2(\frac{\varphi}{2})}\right] \qquad (3)$$

The close form of Equation (3) indicates that a ring resonator in the particular case is very similar to a Fabry-Perot cavity, which has an input and output mirror with a field reflectivity, (1-κ), and a fully reflecting mirror. κ is the coupling coefficient, and $x = \exp(-\alpha L/2)$ represents a roundtrip loss coefficient, $\phi_0 = kLn_0$ and $\phi_{NL} = kLn_2|E_{in}|^2$ are the linear and nonlinear phase shifts, $k = 2\pi/\lambda$ is the wave propagation number in a vacuum. Where L and α are a waveguide length and

linear absorption coefficient, respectively. In this work, the iterative method is introduced to obtain the results as shown in Equation (3), similarly, when the output field is connected and input into the other ring resonators.

After the signals are multiplexed with the generated chaotic noise, then the chaotic cancellation is required by the individual user. To retrieve the signals from the chaotic noise, we propose to use the add/drop device with the appropriate parameters. This is given in details as followings. The optical circuits of ring-resonator add/drop filters for the throughput and drop port can be given by Equations (4) and (5), respectively [9].

$$\left|\frac{E_t}{E_{in}}\right|^2 = \frac{\left(1-\kappa_1\right)-2\sqrt{1-\kappa_1}\cdot\sqrt{1-\kappa_2}e^{-\frac{\alpha}{2}L}\cos\left(k_nL\right)+\left(1-\kappa_2\right)e^{-\alpha L}}{1+\left(1-\kappa_1\right)\left(1-\kappa_2\right)e^{-\alpha L}-2\sqrt{1-\kappa_1}\cdot\sqrt{1-\kappa_2}e^{-\frac{\alpha}{2}L}\cos\left(k_nL\right)} \quad (4)$$

$$\left|\frac{E_d}{E_{in}}\right|^2 = \frac{\kappa_1\kappa_2 e^{-\frac{\alpha}{2}L}}{1+\left(1-\kappa_1\right)\left(1-\kappa_2\right)e^{-\alpha L}-2\sqrt{1-\kappa_1}\cdot\sqrt{1-\kappa_2}e^{-\frac{\alpha}{2}L}\cos\left(k_nL\right)} \quad (5)$$

where E_t and E_d represents the optical fields of the throughput and drop ports respectively. $\beta = kn_{eff}$ is the propagation constant, n_{eff} is the effective refractive index of the waveguide and the circumference of the ring is $L = 2\pi R$, here R is the radius of the ring. In the following, new parameters will be used for simplification: $\phi = \beta L$ is the phase constant. The chaotic noise cancellation can be managed by using the specific parameters of the add/drop device, which the required signals can be retrieved by the specific users. κ_1 and κ_1 are coupling coefficient of add/drop filters, $k_n = 2\pi/\lambda$ is the wave propagation number for in a vacuum, and where the waveguide (ring resonator) loss is α = 0.5 dBmm^{-1}. The fractional coupler intensity loss is γ = 0.1. In the case of add/drop device, the nonlinear refractive index is neglected.

3. Results and Discussion

In operation, the large bandwidth signal within the micro ring device can be generated by using a common soliton pulse input into the nonlinear micro ring resonator. This means that the broad spectrum of light can be generated after the soliton pulse is input into the ring resonator system. The schematic diagram of the proposed system is as shown in **Figure 1**. A soliton pulse with 50 ns pulse width, peak power at 2 W is input into the system. The suitable ring parameters are used, for instance, ring radii R_1 = 15.0 μm, R_2 = 10.0 μm, $R_3 = R_s$ = 5.0 μm and $R_5 = R_d$ = 20.0 μm. In order to make the system associate with the practical device [8], the selected parameters of the system are fixed to λ_0 = 1.55 μm, n_0 = 3.34 (InGaAsP/InP), A_{eff} = 0.50, 0.25 μm^2 and 0.10 μm^2 for a micro ring and nano ring resonator, respectively, α = 0.5 dBmm^{-1}, γ = 0.1. The coupling coefficient (kappa, κ) of the micro ring resonator ranged from 0.1 to 0.95. The nonlinear refractive index is $n_2 = 2.2 \times 10^{-13}$ m^2/W. In this case, the wave guided loss used is 0.5 dBmm^{-1}. The input soliton pulse is chopped (sliced) into the smaller signals spreading over the spectrum (*i.e.*, broad wavelength) as shown in **Figures 2(b)** and **2(g)**, which is shown that the large bandwidth signal is generated within the first ring device. The biggest output amplification is obtained within the nano-waveguides (rings R_3 and R_4) as shown in **Figures 2(d)** and **2(e)**, whereas the maximum power of 10 W is obtained at the center wavelength of 1.5 μm. The coupling coefficients are given as shown in the figures. The coupling loss is included due to the different core effective areas between micro and nano ring devices, which is given by 0.1 dB.

We have shown that a large bandwidth of the optical signals with the specific wavelength can be generated within the micro ring resonator system as shown in **Figure 1**. The amplified signals with broad spectrum can be generated, stored and regenerated within the nano-waveguide. The maximum stored power of 10 W is obtained as shown in **Figures 2(d)** and **2(e)**, where the average regenerated optical output power of 4 W is achieved via and a drop port of an add/drop filter as shown in **Figures 2(h)-2(k)**, which is a broad spectra of light cover the large bandwidth as shown in **Figure 2(g)**. However, to make the system being realistic, the waveguide and connection losses are required to address in the practical device, which may be affected the signal amplification. The storage light pulse within a storage ring (R_s or R_4) is achieved, which has also been reported by Ref. [7]. In applications, the increasing in communication channel and network capacity can be formed by using the different soliton bands (center wavelength) as shown in **Figure 2**, where **2(h)** 0.51 μm, **2(i)** 0.98 μm, **2(j)** 1.48 μm and **2(k)** 2.46 μm are the generated center wavelengths of the soliton bands. The selected wavelength center can be performed by using the designed add/drop filter, where the required spectral width (Full Width at Half Maximum, FWHM) and free spectrum range (FSR) are obtained, the channel spacing and bandwidth are represented by FSR and FWHM, respectively, for in

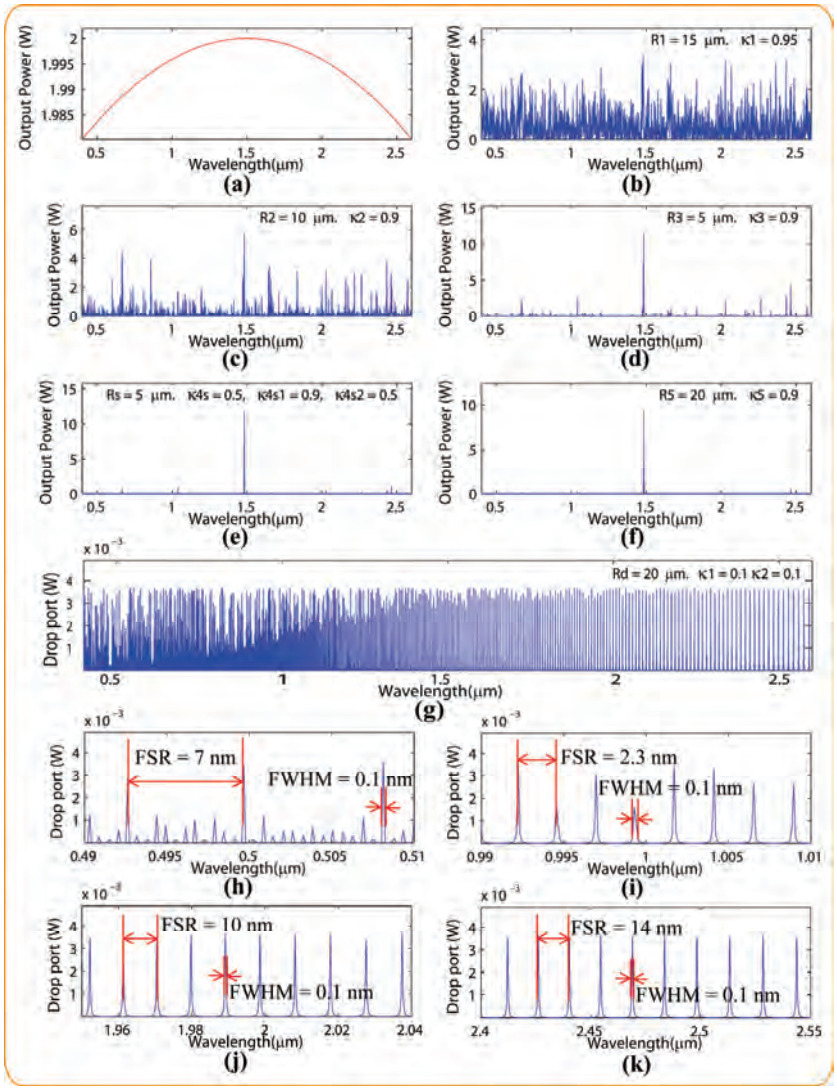

Figure 2. A soliton band with center wavelength at 1.5 μm, where (a) input soliton; (b) ring R_1; (c) ring R_2; (d) ring R_3; (e) storage ring (R_s); (f) ring R_5; (g) drop port output signals. The output of different soliton bands (center wavelength) are as shown, where (h) 0.51 μm; (i) 0.98 μm; (j) 1.99 μm; (k) 2.48 μm.

stance, the FSR and FWHM of 2.3 nm and 100 pm are obtained as shown in **Figure 2(i)**.

4. Conclusions

In conclusion, apart from communication application, the idea of personnel wavelength (network) being realistic for the large demand user due to un-limit wavelength discrepancy, whereas the specific soliton band can be generated using the proposed system. The potential of soliton bands such as visible soliton (color soliton), UV-soliton, X-ray soliton and infrared soliton can be generated and used for the applications such as multi color holography, medical tools, security imaging and transparent holography and detection, respectively.

5. Acknowledgements

One of the authors (Muhammad Arif Jalil) would like to acknowledge Nanoscale Science and Engineering Research Alliance (N'SERA), King Mongkut's Institute of Technology Ladkrabang, Bangkok (KMITL), Thailand for research facility, and he would also like to extend his appreciation to UTM for funding this research work.

6. References

[1] N. Pornsuwancharoen, U. Dunmeekaew and P. P. Yupapin, "Multi-Soliton Generation Using a Micro Ring Resonator System for DWDM Based Soliton Communication," *Microwave and Optical Technology Letters*, Vol.

51, No. 5, 2009, pp. 1374-1377.

[2] P. P. Yupapin, N. Pornsuwanchroen and S. Chaiyasoonthorn, "Attosecond Pulse Generation Using Nonlinear Micro Ring Resonators," *Microwave and Optical Technology Letters*, Vol. 50, No. 12, 2008, pp. 3108-3011.

[3] N. Pornsuwancharoen and P. P. Yupapin, "Generalized Fast, Slow, Stop, and Store Light Optically within a Nano Ring Resonator," *Microwave and Optical Technology Letters*, Vol. 51, No. 4, 2009, pp. 899-902.

[4] N. Pornsuwancharoen, S. Chaiyasoonthorn and P. P. Yupapin, "Fast and Slow Lights Generation Using Chaotic Signals in the Nonlinear Micro Ring Resonators for Communication Security," *Optical Engineering*, Vol. 48, No. 1, 2009, p. 50005-1-5.

[5] P. P. Yupapin, P. Saeung and C. Li, "Characteristics of Complementary Ring-Resonator Add/Drop Filters Modeling by Using Graphical Approach," *Optics Communications*, Vol. 272, No. 1, 2007, pp. 81-86.

[6] M. Fujii, J. Leuthold and W. Freude, "Dispersion Relation and Loss of Subwavelength Confined Mode of Metal-Dielectri-Gap Optical Waveguides," *IEEE Photonics Technology Letters*, Vol. 21, No. 6, 2009, pp. 362-364.

[7] P. P. Yupapin and N. Pornsuwancharoen, "Proposed Nonlinear Micro Ring Resonator Arrangement for Stopping and Storing Light," *IEEE Photonics Technology Letters*, Vol. 21, No. 6, 2009, pp. 404-406.

[8] Y. Su, F. Liu and Q. Li, "System Performance of Slow-light Buffering and Storage in Silicon Nano-Waveguide," *Proceedings of SPIE*, Vol. 6783, 2007, p. 67832.

[9] P. P. Yupapin and W. Suwancharoen, "Chaotic Signal Generation and Cancellation Using a Micro Ring Resonator Incorporating an Optical Add/Drop Multiplexer," *Optics Communications*, Vol. 280, No. 2, 2007, pp. 343-350.

ISSN: 2153-1285 Vol.1, No.2, October 2010

Scientific Research

Circuits and Systems

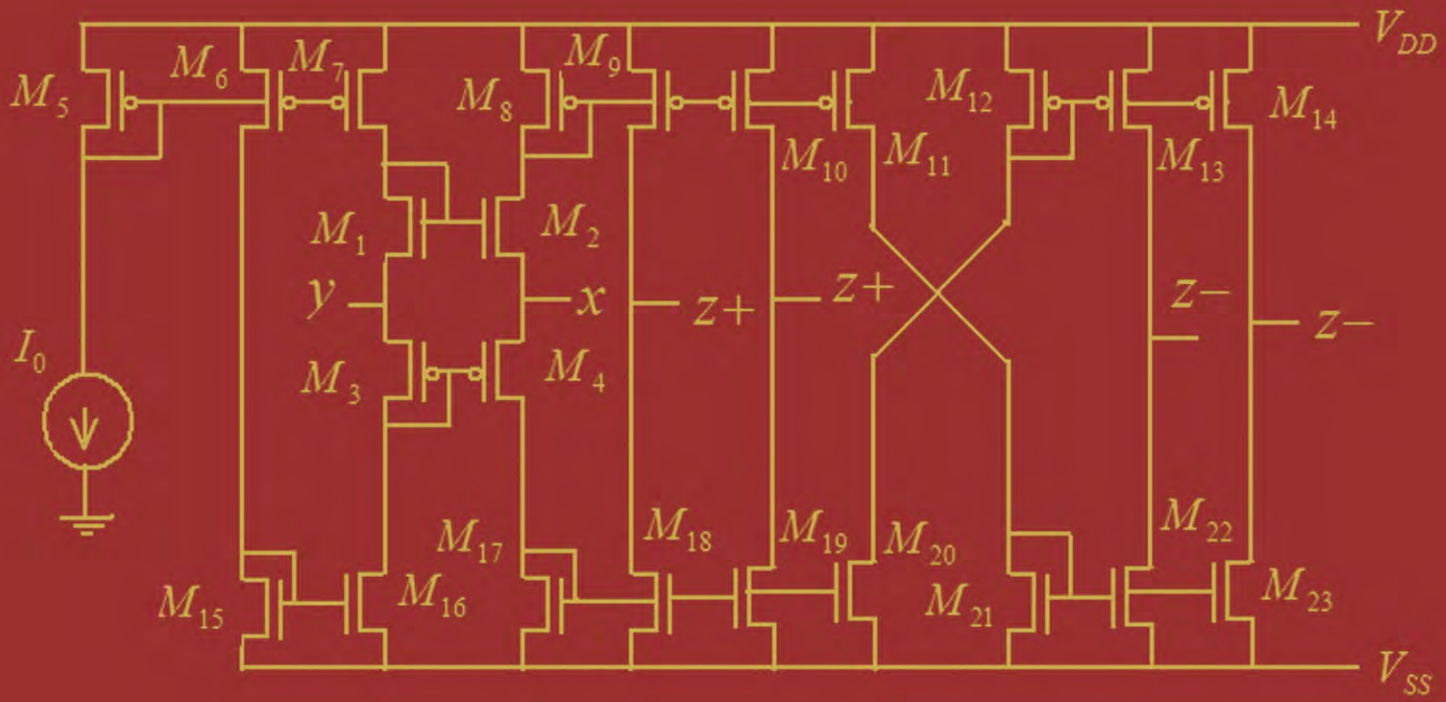

ISSN: 2153-1285

www.scirp.org/journal/cs

Journal Editorial Board

ISSN 2153-1285 (Print) ISSN 2153-1293 (Online)

http://www.scirp.org/journal/cs

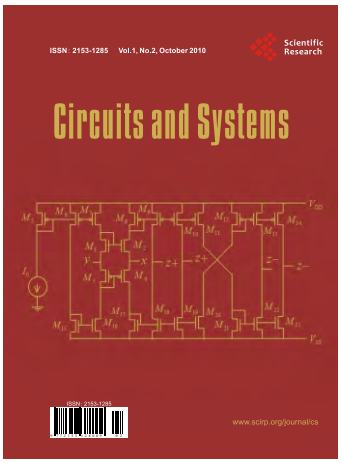

Call for Papers

Circuits and Systems

ISSN Print: 2153-1285 ISSN Online:2153-1293

http://www.scirp.org/journal/cs

Circuits and Systems is an international journal dedicated to the latest advancement of theories, methods and applications in Electronics, Circuits and Systems. The goal of this journal is to provide a platform for scientists and academicians all over the world to promote, share, and discuss various new issues and developments in different areas of electronics, circuits and systems.

Subject Coverage

All manuscripts must be prepared in English, and are subject to a rigorous and fair peer-review process. Accepted papers will immediately appear online followed by printed hard copy. The journal publishes original papers including but not limited to the following fields:

- Analog Signal Processing
- Biomedical Circuits and Systems
- Blind Signal Processing
- Cellular Neural Networks and Array Computing
- Circuits and Systems for Communications
- Computer-Aided Network Design
- Digital Signal Processing
- Graph Theory and Computing
- Life-Science Systems and Applications
- Live Demonstrations of Circuits and Systems
- Multimedia Systems and Applications
- Nanoelectronics and Gigascale Systems
- Neural Systems and Applications
- Nonlinear Circuits and Systems
- Power Systems and Power Electronic Circuits
- Sensory Systems
- Visual Signal Processing and Communications
- VLSI Systems and Applications

We are also interested in: 1) Short Reports 2-5 page papers where an author can either present an idea with theoretical background but has not yet completed the research needed for a complete paper or preliminary data; 2) Book Reviews Comments and critiques.

Notes for Intending Authors

Submitted papers should not have been previously published nor be currently under consideration for publication elsewhere. Paper submission will be handled electronically through the website. All papers are refereed through a peer review process. For more details about the submissions, please access the website.

Website and E-Mail

http://www.scirp.org/journal/cs E-mail:cs@scirp.org

Circuits and Systems, 2010, 1, 35-75
Published Online October 2010 in SciRes (http://www.SciRP.org/journal/cs).

TABLE OF CONTENTS

Volume 1 Number 2 **October 2010**

